ISTANBUL TECHNICAL UNIVERSITY ★ GRADUATE SCHOOL OF SCIENCE ENGINEERING AND TECHNOLOGY

COPPER – DIAMOND COMPOSITE FABRICATION BY ELECTROFORMING PROCESS FOR THERMAL MANAGEMENT APPLICATIONS

M.Sc. THESIS

Gökçe EVREN

Department of Metallurgical and Materials Engineering

Materials Engineering Programme

JULY 2020

ISTANBUL TECHNICAL UNIVERSITY ★ GRADUATE SCHOOL OF SCIENCE ENGINEERING AND TECHNOLOGY

COPPER – DIAMOND COMPOSITE FABRICATION BY ELECTROFORMING PROCESS FOR THERMAL MANAGEMENT APPLICATIONS

M.Sc. THESIS

Gökçe EVREN
(506171413)

Department of Metallurgical and Materials Engineering

Materials Engineering Programme

Thesis Advisor: Prof. Dr. Mustafa ÜRGEN

JULY 2020

ISTANBUL TEKNİK ÜNİVERSİTESİ ★ FEN BİLİMLERİ ENSTİTÜSÜ

ELEKTROŞEKİLLENDİRME İLE ÜRETİLEN ISIL YÖNETİM AMAÇLI BAKIR – ELMAS KOMPOZİT KAPLAMALAR

YÜKSEK LİSANS TEZİ

Gökçe EVREN
(506171413)

Metalurji ve Malzeme Mühendisliği Ana Bilim Dalı

Malzeme Mühendisliği Programı

Tez Danışmanı: Prof. Dr. Mustafa ÜRGEN

TEMMUZ 2020

Gökçe EVREN, a M.Sc. student of ITU Graduate School of Science Engineering and Technology student ID 506171413, successfully defended the thesis entitled "COPPER – DIAMOND COMPOSITE FABRICATION BY ELECTROFORMING PROCESS FOR THERMAL MANAGEMENT APPLICATIONS", which she prepared after fulfilling the requirements specified in the associated legislations, before the jury whose signatures are below.

Thesis Advisor :	**Prof. Dr. Mustafa ÜRGEN** Istanbul Technical University	....
Jury Members :	**Asst. Prof. Dr. Nuri SOLAK** Istanbul Technical University	....
	Asst. Prof. Dr. Fatma BAYATA Istanbul Bilgi University	....

Date of Submission : 08 June 2020
Date of Defense : 07 July 2020

to my family,

FOREWORD

I would like to express my sincere appreciation to my thesis advisor Prof. Dr. Mustafa ÜRGEN for his endless guidance in the light of his extensive knowledge and enthusiasm for science.

I would also like to thank Prof. Dr. Hüseyin ÇIMENOĞLU, Asst. Prof. Nuri SOLAK and members of their research groups.

I am very grateful to Res. Asst. Burçak AVCI, Res. Asst. Çağatay YELKARASI, Res. Asst. Erkan KAÇAR, Seyhan ATIK and Sevgin TÜRKELI. Whenever the need arises, you were always there.

Words are powerless to express my graditude to my dear husband Res. Asst. Burak EVREN. Thank you for always being there for me.

The last but not the least I would like to thank to the ones, who have always supported me from the very beginning of my life. My precious mother Tülay, my dear father Ahmet, my one and only brother Can and my grandmother Müşerref. Thank you for raising me into the person who I am today.

July 2020 Gökçe EVREN
(Res. Asst.)

TABLE OF CONTENTS

Page

FOREWORD .... **ix**
TABLE OF CONTENTS .... **xi**
ABBREVIATIONS .... **xiii**
SYMBOLS .... **xv**
LIST OF TABLES .... **xvii**
LIST OF FIGURES .... **xix**
SUMMARY .... **xxi**
ÖZET .... **xxiii**
1. INTRODUCTION **1**
2. LITERATURE OVERVIEW **3**
  2.1 Heat Transfer and Thermal Conductivity 3
    2.1.1 Thermal management 3
      2.1.1.1 Active thermal management 3
      2.1.1.2 Passive thermal management 4
    2.1.2 Heat transfer 6
    2.1.3 Thermal conductivity 7
      2.1.3.1 Thermal conductivity of metals 8
      2.1.3.2 Thermal conductivity of ceramics 9
      2.1.3.3 Thermal conductivity of polymers 10
    2.1.4 Thermal expansion 10
      2.1.4.1 Material selection for thermal management applications 10
  2.2 Composite Materials 12
  2.3 Production Methods of MMCs 13
    2.3.1 Liquid state production methods 13
      2.3.1.1 Stir casting 13
      2.3.1.2 Infiltration method 14
    2.3.2 Solid state production methods 17
      2.3.2.1 Powder metallurgy 17
      2.3.2.2 Sinter forging 18
      2.3.2.3 Diffusion bonding 18
    2.3.3 Spray deposition 19
    2.3.4 Electrochemical composite fabrication 20
    2.3.5 History of composite electrodeposition 27
    2.3.6 Sediment codeposition 29
    2.3.7 Previous studies on SCD 29
3. EXPERIMENTAL STUDIES **33**
  3.1 Electroforming System Design 33
  3.2 Experimental Procedure 37
  3.3 Results & Discussion 39
    3.3.1 Process optimization 39
    3.3.2 Surface imaging of as deposited samples 46
    3.3.3 Surface imaging of post treated samples 50

3.3.4 Structural characterization 55
3.3.5 Mechanical characterization...58
4. CONCLUSION..61
REFERENCES..63
CURRICULUM VITAE...69

ABBREVIATIONS

BSE : Back-Scattered Electrons
CED : Conventional Electrodeposition
CIP’d : Cold Isostatic Pressed
CTE : Coefficient of Thermal Expansion
DC : Direct Current
EDS : Energy Dispersive X-Ray Spectroscopy
GPI : Gas Pressure Infiltration
CTE : Coefficient of Thermal Expansion
EDS : Energy Dispersion Spectroscopy
GPI : Gas Pressure Infiltration
MMC : Metal Matrix Composite
PDI : Pressure Die Infiltration
RE : Reference Electrode
SC : Standard Conditions
SCD : Sediment Codeposition
SE : Secondary Electrons
SEM : Scanning Electron Microscope
WE : Working Electrode
XRD : X-Ray Diffraction

SYMBOLS

F : Faraday constant
h : Convective heat transfer coefficient
l_f : Final length
l_0 : Initial length
i_a : Anodic current density
i_c : Cathodic current density
i_0 : Exchange current density
k : Thermal conductivity
Q : Rate of heat transfer
t : Time
T : Temperature
R : Gas constant
t : Time
T : Temperature
T_f : Final temperature
T_0 : Initial temperature
x : Distance
z : Valance
α : Linear coefficient of thermal expansion
ε : Emissivity
η : Overpotential
η_d : Activation overpotential
σ : Radiant heat transfer coefficient

LIST OF TABLES

Page

Table 2.1 : Thermal properties of various metals under standard conditions **8**
Table 2.2 : Thermal properties of various ceramic materials at SC. **9**
Table 3.1 : Copper-diamond composite electroforming bath. **37**
Table 3.2 : Optimized operation parameters of copper-diamond electroforming. **38**
Table 3.3 : Diffraction planes and corresponding angles for characterized samples.**57**

LIST OF FIGURES

Page

Figure 2.1 : Heat sink attached on a circuit board. **5**
Figure 2.2 : Thermal conductivity and CTE values of certain materials. **11**
Figure 2.3 : Stir casting process illustration.. **14**
Figure 2.4 : Illustration of Gas Pressure Infiltration (GPI) Technique. **15**
Figure 2.5 : Illustration of Pressure Die Infiltration (PDI) technique. **16**
Figure 2.6 : Illustration of Squeeze Casting Infiltration technique. **16**
Figure 2.7 : Compaction stage of powder mixture... **18**
Figure 2.8 : Illustration of diffusion bonding method. **19**
Figure 2.9 : Illustration of spray deposition technique. **19**
Figure 2.10 : Wettability of a liquid, wetting angle smaller than 90° (left), larger than 90° (right). **20**
Figure 2.11 : DC electrolysis system. **22**
Figure 2.12 : Movement of ions through the electrolyte... **24**
Figure 2.13 : Relation of current density with potential. **25**
Figure 2.14 : Sediment codeposition setup illustration... **29**
Figure 3.1 : Compartments of the cathode system. **34**
Figure 3.2 : Sequence of assembly for the cathode system. **35**
Figure 3.3 : Illustration of the experimental setup. **36**
Figure 3.4 : Copper-diamond electroforming setup. **37**
Figure 3.5 : Settled diamond particles inside the hole on the designed cathode system (left), samples from the first electroforming attempt (right). ... **40**
Figure 3.6 : Diamond particle clusters floating on the electrolyte surface. **40**
Figure 3.7 : Usage of pre-wet diamond particles. **41**
Figure 3.8 : First set of samples formed by using wet diamond particles................. **41**
Figure 3.9 : SEM images of copper-diamond composite cross-section at 35X mag. with secondary electrons (left) and back-scattered electrons (right). ... **42**
Figure 3.10 : Three electrode cell (left) filled with electroforming bath to plot the polarization curve with potentiostat (right). **43**
Figure 3.11 : Polarization curve plotted in process bath indicating regions where I: Activation controlled, II: Mixed controlled, III: Diffusion controlled. **44**
Figure 3.12 : Macroscopic and optical microscope image of sample fabricated with potential controlled system **44**
Figure 3.13 : Characterization of the first sample fabricated by potential controlled system; a) SEM image of surface with SE at 35X mag. (b) EDS analysis, (c,d) SEM images of cross-section with SE at 35X, 75X mag. **45**
Figure 3.14 : Lifting the composite from substrate.. **46**
Figure 3.15 : SEM images of sample surface with 250 µm diamond particles; (a,b) at 200X with SE, BSE respectively, (c,d) at 1kX with SE, BSE respectively. **47**

Figure 3.16 : SEM images of sample cross-sections with 250 µm diamond particles; (a,b) at 50X with SE, BSE respectively, (c,d) at 100X with SE, BSE respectively. **48**
Figure 3.17 : SEM images of sample cross-sections with 75 µm diamond particles; (a,b) at 100X with SE, BSE respectively, (c,d) 30° tilted at 750X, 200X with SE, BSE respectively. **49**
Figure 3.18 : SEM images of annealed samples cross-section; (a,b) 250 µm particles at 150X with SE, BSE resp. (c,d) 75 µm particles at 150X with SE, BSE resp. (e,f) 75 µm particles at 1kX with SE, BSE resp. **50**
Figure 3.19 : SEM images of CIP'd samples cross-sections with 250 µm particles, (a,b) at 35X with SE, BSE resp. (c,d) at 100X with SE, BSE resp. (e,f) at 350 X with SE, BSE resp. **51**
Figure 3.20 : SEM images of CIP'd samples cross-sections with 75 µm particles, (a,b) at 35X with SE, BSE resp. (c,d) at 200X with SE, BSE resp. (e,f) at 350 X with SE, BSE resp. (g,h) at 500X with SE, BSE resp. **52**
Figure 3.21 : SEM images of CIP'd & annealed samples cross-sections, (a,b) at 100X with SE,BSE resp. (c,d) at 350X with SE, BSE resp. (e,f) at 100X with SE, BSE resp. (g,h) at 350X with SE, BSE resp. **54**
Figure 3.22 : XRD pattern of copper – diamond coating on copper substrate after 6 hours electroforming. **55**
Figure 3.23 : XRD patterns of as deposited, as annealed, as CIP'd and as initially CIP'd then annealed sample (combined) plotted in gonio mode. **56**
Figure 3.24 : Three point flexural test results of as deposited and as annealed samples. **58**

COPPER – DIAMOND COMPOSITE FABRICATION BY ELECTROFORMING PROCESS FOR THERMAL MANAGEMENT APPLICATIONS

SUMMARY

Challenge in today’s electronics world is miniaturization of electronic packages with suitable thermal management. Resistance against the conduction of electrons in electronic circuits causes heat generation. Generated heat should be dissipated quickly and reliably, or else device will encounter overheating related failures. Thermal management applications deals with heat dissipation. Simplest and most commonly applied thermal management method is conduction of the generated heat to air by means of a thermally conductive material, which is attached on heat generating component. For that purpose heat sinks or heat spreaders are commonly used in thermal management applications. Currently used heat sink materials are aluminum and copper; however, their usage in thermal management has a significant drawback that cannot be neglected. Despite being one of the highest thermally conductive metals, coefficient of thermal expansion (CTE) of copper is higher than the CTE of semiconductor on which heat sink is attached. For reliable heat dissipation and prevention of possible incompatible elongation related fractures, CTE of semiconductor material and heat sink material should match.

Copper has a thermal conductivity of 398 W/m^{-1}.K^{-1} and CTE of 17.10^{-6}K.$^{-1}$. Despite having satisfactory thermal conductivity, its CTE value is almost three times that of the semiconductor material. When copper is produced in composite form with diamond particles as reinforcement phase, not only a reduced CTE value is achieved, also an increased thermal conductivity is obtained. By adjusting the volume fraction of phases which constitute a composite material, material properties can also be adjusted. Diamond here is the reinforcing material of choice since having a thermal conductivity higher than 2000 W.m^{-1}.K^{-1}, highest among all known materials, and a CTE value of 1.1.10^{-6}.K^{-1} makes diamond a unique material for thermal management applications.

In this thesis, copper-diamond composite material to be used in thermal management applications is produced by electrochemical deposition method. Rather than conventional electrodeposition techniques, a modified sediment codeposition method is used. Particular electroforming system is designed for production of a near net shape and self-standing composite material.

As electroforming electrolyte, traditional acidic copper sulfate plating bath containing 180 g/l copper sulfate, 30 g/l sulfuric acid, 0.1 g/l hydrochloric acid and 0.05 g/l Thiouera is prepared. 75 µm and 250 µm diamond particles are utilized in the codeposition process. Initial set of experiments are conducted without particles for optimization of operating conditions. After with optimized parameter smooth and bright copper is obtained, diamond is incorporated in copper matrix. First set of experiments are conducted 2-4 hours with 250 µm diamond particles. Particles are wetted in an electrolyte having identical composition with forming electrolyte prior to

electroforming. Prior to electrodeposition process cathodic polarization curve is obtained potentiodynamically and the substrate surface potential required to be applied, corresponding to current density of 1 A/dm^2, is derived from the polarization plot. As the deposit fills up the gaps between particles and grows further, available cathodic area changes. For that reason current density controlled deposition is not feasible. Therefore experiments were conducted potential controlled.

Further experiments are conducted by optimized parameters with duration of 30 hours for copper to cover the particles entirely. After the surface coverage with homogeneous distribution of particles in matrix is obtained, reproducibility of method is examined using diamond particles with particle sizes of 75 and 250 µm. Annealing and cold isostatic pressing are applied for an improved copper-diamond interface. A group of samples are annealed for 2 hours at 650 °C, another group of samples are cold isostatic pressed for 10 minutes under the pressure of 1.5 x 10^6 N, a group of samples are both annealed and CIP’ed. Distribution of diamond particles, copper-diamond interface and morphology of copper deposit are investigated by Scanning Electron Microscopy. After cold isostatic pressing it is observed that copper morphology changed itself to an indented structure from a smooth morphology.

X-Ray Diffraction patterns of samples with 75 µm diamond particles are plotted to investigate structural properties of as deposited samples and for observation of changes induced by annealing, cold isostatic pressing and both annealing and cold isostatic pressing. As deposited samples have copper peaks slightly shifted to smaller angles in respect of induced compression stresses while deposition. For annealed samples shifting to higher angles with a large extend is obtained. Cold isostatic pressing shifted the angles to smaller values. Copper peaks at smaller angles are also for the samples both exposed to cold isostatic pressing and annealing observed.

Three point flexural test is conducted to as deposited and annealed samples to observe how mechanical properties are effected by annealing. Flexural strength test results indicated that flexural strength of copper-diamond composite is lowered by annealing. Flexural strength of annealed sample is 1.2 MPa while for as deposited sample it is 2.8 MPa. When there is a need for increased ductility regarding further forming processes material can be annealed.

Copper-diamond composites produced with electroforming technique in desired shape and dimensions with enhanced diamond content. Material has void free structure and reliable interface.

ELEKTROŞEKİLLENDİRME İLE ÜRETİLEN ISIL YÖNETİM AMAÇLI BAKIR ELMAS KOMPOZİT KAPLAMALAR

ÖZET

Elektronik cihazların performansını önemli ölçüde etkileyen bir unsur olan aşırı ısınma, teknolojinin ilerlemesi önünde engel teşkil etmektedir. Elektronik alanında yapılan çalışmalarda son yıllarda eğilim küçük boyutlarda ve yüksek performansta çalışan cihazların tasarlanması yönündedir. Arzu edilen niteliklere sahip cihazların kullanımı ısıl yönetim olmadan mümkün olmamakta, cihaz tasarımlarındaki minimalist eğilim ise ısıl yönetimi güç kılmaktadır.

Elektrik iletimi esnasında akıma gösterilen direnç sebebi ile açığa çıkan ısı, cihazdan aktif ya da pasif ısıl yönetim prensipleri ile uzaklaştırılır. Aktif ısıl yönetim türleri; çalışırken dış enerji kaynağına ihtiyaç duymalar, pasif yöntemlere kıyasla karmaşık şekillerde bulunmaları, yüksek maliyetli tasarımlar olmaları ve çalışma esnasında ses üretmeleri gibi dezavantajlara sahiptirler. Fanlar, termoelektrik soğutucular, sıvı soğutma sistemleri aktif yöntemlerdir ve çalışma esnasında ses üretmektedirler. Pasif yöntemler üretilen ısının cihazdan uzaklaştırılmasında ve/veya ısı üreten parçadan aktif soğutucu elemana ısı aktarımında kullanılır. En çok kullanılan ısıl yönetim türleri pasif soğutma yöntemlerinden olan ısı muslukları ve ısı dağıtıcılardır. Her iki yüzeyi düz yapıya sahip ısı dağıtıcıların ve bir yüzeyi düz diğer yüzeyi hava ile teması artıracak biçimde tasarlanmış kanatlı bir yapıda bulunan ısı musluklarının çalışma prensibi ısının yüksek sıcaklık kaynağından düşük sıcaklıktaki ortama kondüksiyon yolu ile aktarılmasına dayanır.

Isıl yönetim amaçlarına yönelik uygulamalarda kullanılmakta olan soğutucu malzemeler arasında en yaygın kullanılan malzemeler bakır ve alüminyumdur. Bakırın ısıl iletkenliği 398 $W.m^{-1}.K^{-1}$ değeri ile alüminyumun ısıl iletkenliğinden çok daha yüksektir. Böylece bakır ısıl yönetim uygulamalarında soğutucu olarak kullanılmak üzere alüminyumdan daha başarılı bir aday olmaktadır. Ancak bakır soğutucuların kullanımı beklenildiği kadar güvenilir sonuç vermemektedir. Bu durumun altında yatan sebep irdelendiğinde; bakır soğutucu ile soğutucunun üzerine monte edildiği yarıiletken malzemenin ısıl iletkenlik katsayıları arasında büyük bir fark olması, bu nedenle ısınma ve soğuma çevrimleri esnasında farklı ölçülerde uzama sonucu ortaya çıkan eğilip bükülmeler nedeniyle bu parçaların arasındaki kontakta temassızlıklar meydana gelmesi yer alır. Temassızlık durumunda ise güvenilir bir soğutmaya ulaşılması mümkün olamaz, malzemede üretilen ısı uzaklaştırılamaz ve lokal olarak başlayıp tüm cihaza yayılabilecek aşırı ısınma sorunuyla karşılaşılır. Malzemeler arasındaki ısıl iletkenlik farkının yüksek ısıl iletkenlikten ödün verilmeden birbirine yakın değerlerde olması gerekmektedir. Üzerinde yer aldığı elektronik parçanın ısıl iletkenliğine uyumlu ısıl genleşme katsayısına sahip mevcut malzemeler, ısıl iletkenliklerinin düşük olmaları sebebiyle ısıl yönetim uygulamalarında kullanılmaları mümkün olamamaktadır.

Bakırın çeşitli malzemelerle alaşımlanması ile ısıl iletkenliğinin düşürülmesine yönelik çalışmalar yapılmış, ancak elde edilen ısıl iletkenlik değerleri yetersiz olmuştur. Son yıllarda yapılan çalışmalarda farklı malzemelerin sahip olduğu özellikler bir araya getirilerek üstün özelliklere sahip kompozit malzeme üretimi, ısıl iletkenlik uygulamalarında da kullanılarak bakırın çeşitli malzemelerle takviyelendirilmesi ile ısıl iletkenlik değerini düşürmeden ısıl genleşme katsayısının azaltılması başarılı bir şekilde sağlanmıştır. Bakır matrisli kompozit malzemede kullanılacak olan takviye malzemesinin sahip olması gereken özellikler yüksek ısıl iletkenlik ve düşük ısıl genleşme katsayısıdır.

Elmas 2000 $W.m^{-1}.K^{-1}$ üzerindeki yüksek ısıl iletkenliğe ve yaklaşık $1.10^{-6}.K^{-1}$ değerinde düşük ısıl genleşme katsayısına sahip olması sebebiyle bakırın takviyelendirilmesinde kullanılmaktadır. Bakır-elmas kompozit üretiminde kullanılan bakır matrisin üretim aşamasında sıvı fazda bulunduğu infiltrasyon ve katı fazda bulunduğu toz metalürjisi yöntemlerinde, bakır matris ile elmas partikülleri arasındaki ıslanma problemi sebebiyle sağlam bir ara yüzey elde edilememektedir. Ara yüzey, termal bariyer oluşturarak malzemenin ısı iletimini olumsuz etkilemektedir. İnfiltrasyon ve toz metalurjisi yöntemleri ile yeterli özelliklere sahip ara yüzeyin elde edilememesi sebebiyle teorik olarak hesaplanan değerin altında ısıl özelliklere sahip malzemeler elde edilmektedir. Ara yüzeyin iyileştirmesine yönelik matrisin alaşımlandırılması, karbür yapıcı elementlerin ilavesi, elmas partiküllerin yüzey özelliklerinin değiştirilmesi gibi çözümler kullanılmaktadır. Ancak bu çözüm yolları yüksek sıcaklık, basınç, inert atmosfer gerektiren üretim yöntemlerine ilave prosesler eklemekte ve maliyeti artırmaktadır.

Metal matrisli kompozitlerin katı ve sıvı fazlı üretim yöntemlerinde mevcut olan dezavantajların, temelde yüksek proses sıcaklıklarına olan ihtiyaçtan kaynaklanmakta olduğu düşünüldüğünde; işlem sıcaklığının oda sıcaklığına yakın değerlerde olduğu elektrokimyasal yöntem ile kompozit üretimi ümit vadeden bir alternatif oluşturmaktadır.

Bu çalışmada, ısıl yönetim uygulamalarında kullanıma yönelik bakır-elmas kompozitinin elektroşekillendirme yöntemi üretimi gerçekleştirilmiştir. Elektrokimyasal yöntemle kompozit üretiminde yüksek hacimsel takviye oranlarına ulaşmak amacıyla kullanılan sediment biriktirme yönteminin modifiye edilerek kullanılmasıyla, bakır 75 µm ve 250 µm boyutlardaki elmas partikülleri ile takviyelendirilmiştir.

Elektroşekillendirme elektrolit çözeltisi olarak 180 g/l bakır sülfat, 30 g/l sülfürik asit ve 0,1 g/l hidroklorik asit içeren geleneksel asidik bakır kaplama banyosu hazırlanmış, parlatıcı olarak 0,05 g/l tüyoüre kullanılmıştır. Elektrot olarak bakır anot ve bakır katot kullanılmış, öncelikli olarak bakır elektroşekillendirme parametreleri takviye kullanılmadan optimize edilmiştir.

Çalışmada katot ve anot sediment biriktirme yöntemlerindeki gibi yatay pozisyonda konumlanmış ve geleneksel sediment biriktirme yöntemlerinden farklı olarak, arzu edilen son şekil ve boyutlarda kompozit malzeme üretimini mümkün kılmak amacıyla katot üzerine monte edilen bir kapak tasarlanmıştır. Kapağın üst kısmında bulunan delik sayesinde yalnızca istenilen boyut ve şekildeki alan çözelti ile temas etmektedir. Bu deliğin içerisine elmas partikülleri konumlandırılır ve sisteme akım verilerek bakır matrisin elmas partikülleri arasındaki boşlukları dolduracak şekilde birikimi başlar.

Elmas partiküller altlık yüzeyine yerleştirilmeden önce, aglomerasyonu önlemek amacı ile elektroşekillendirme banyosu ile aynı kompozisyona sahip bir çözeltide ıslatılmıştır. Tasarlanan sistem ve optimize edilen parametreler ile, altlık yüzeyine konumlandırılan 250 µm boyutlu elmas partikülleri kullanılarak 2-4 süre ile biriktirme işlemi gerçekleştirilmiştir. Ancak istenilen morfolojide ve parlak bakır yerine dentritik bakır elde edilmesi akım yoğunluğunun olması gereken aralıktan daha yüksek olduğunu göstermiştir. Partiküller arasındaki boşlukları doldurarak büyüyen bakırın yüzey alanında sürekli bir değişim olması birikime müsait alanı değiştireceğinden akım yoğunluğu kontrollü deneyler uygulanabilir olmamış, potansiyel fark kontrollü deneyler için polarizasyon eğrisi çizilmiştir. Polarizasyon eğrisinde 1 A/dm2 akım yoğunluğuna karşılık gelen potansiyel fark 160 mV olarak ölçülüp, deneyler potansiyel kontrollü yürütülmüştür.

75 ve 250 µm elmas partikülleri ile 30 saat süre ile bakır birikimi gerçekleştirilmiş ve 700 µm üzerinde kalınlıkta malzeme elde edilmiştir. Üst yüzeyden bakıldığında tüm yüzeyde yalnızca bakır görülecek şekilde partiküllerin üzeri bakır ile kaplanmış ve yöntemin tekrarlanabilirliği test edilmiştir. Elektroşekillendirme yöntemi ile üretilen kompozit malzeme, az miktarda manuel kuvvet yardımı ile altlık malzemeden ayrılabilmektedir.

Tavlama, soğuk izostatik presleme ve her iki işlem birlikte uygulanarak ara yüzeye etkileri incelenmiştir. Tavlama prosesi 650 °C'de 2 saat süre ile, soğuk izostatik presleme ise 1,5 x 10^6 N basınç altında 10 dakika süre ile gerçekleştirilmiştir. Her iki işlemin uygulandığı numuneler önce preslenip sonra tavlanmıştır.

Taramalı elektron mikroskobu ile elmas partiküllerin dağılımı, kompozitin arayüzeyi ve bakır morfolojisi incelenmiştir. Soğuk izostatik preslenen numunelerde bakır morfolojisinin iğnesel bir yapıya dönüştüğü gözlemlenmiştir.

X-Işını Difraktometresi ile işlemlerin yapıya etkisi irdelenmiştir. Herhangi bir işlem görmemiş numunelerde bakır pikleri, elektrokimyasal birikim esnasında ortaya çıkan basma gerilmeleri sebebi ile küçük açılara kaymıştır. Tavlanmış numunelerde kayma büyük açılar yönünde, soğuk preslenmiş numunelerde küçük açılar yönünde olmuştur. Soğuk presleme sonrası tavlanan numunelerde bakır piklerinde yine küçük açılar yönünde kayma gözlenmiştir.

Üç noktalı eğme testi ile işlem görmemiş ve tavlanmış numunelerin eğme dayanımları kıyaslanmıştır. Eğme testi sonuçlarında tavlama işleminin eğme dayanımını azalttığı görülmüştür. Tavlanmış numunenin eğme dayanımı 1,2 MPa, işlem görmemiş numunenin eğme dayanımı 2,8 MPa ölçülmüştür.

Malzeme, sünekliğin artırılmasına ihtiyaç duyulan uygulamalarda tavlama işlemi uygulanarak kullanılabilir, tavlama işlemi ile elektrokimyasal biriktirme sırasında ortaya çıkan basma gerilmeleri kaldırılmıştır. Soğuk izostatik presleme sonrası tavlanmış numunelerde soğuk izostatik presleme etkisi malzeme tavlandığında tamamıyla ortadan kalkmamaktadır.

Yüksek takviyeli bakır-elmas kompozit malzeme elektroşekillendirme yöntemi ile arzu edilen şekil ve büyüklüklerde sağlam bir ara yüzey ile boşluksuz yapıda üretilerek, üretimi sonrası kullanıma yönelik uygulanacak şekillendirme yöntemlerine göre soğuk izostatik presleme ve tavlama işlemlerine tabi tutularak ya da malzemeye hiçbir işlem uygulanmadan kullanılabilir.

1. INTRODUCTION

Heat is generated when electronic devices operate. In order to preserve the reliability and performance of the device and to prevent failures, generated heat required to be dissipated quickly [1]. Generally, heat sinks or heat spreaders are heat dissipating components used for thermal management applications in electronics. Heat spreaders are required to have high thermal conductivity since objective is transferring the generated heat to a fluid media. Currently in use heat spreaders are made of high thermal conductivity materials however coefficient of thermal expansion (CTE) of that materials are very different than CTE of semiconductor material. Difference in CTE values cause uneven elongations between semiconductor and heat spreaders and consequently ends up with fracture [2].

Aluminum and copper are the most commonly used conducting materials; moreover, copper has the second greatest thermal conductivity among all metals. However CTE of copper is almost four times of the CTE of semiconductor material [3].

CTE of copper can be reduced by reinforcing with another material. But the consideration is this material should not decrease thermal conductivity. Diamond is an exceptional material and its thermal conductivity has the highest value among all other materials. Reinforcing copper with diamond decreases CTE of copper and increases thermal conductivity at the same time. The production methods used to produce copper-diamond composite material pose problems such as weak bonding between copper matrix and diamond particles and high energy consumption while production. With electrochemical method which requires low operating temperature, diamond particles can be incorporated into copper matrix with a strong interface. Sediment codeposition (SCD) technique enables deposition of reinforcing phase with volumetric concentrations above 50 % vol [4]. In this thesis, diamond particles are incorporated in copper matrix by using a modified SCD technique. Microstructure and thermal properties are analyzed, the effect of annealing and cold isostatic pressing on properties are investigated.

2. LITERATURE OVERVIEW

2.1 Heat Transfer and Thermal Conductivity

2.1.1 Thermal management

In electronic components when current passes through, resistance against conduction causes heat generation. Generated heat should be dissipated quickly. If temperature rises excessively or components are being opposed high localized temperatures, functionality and operational life of the device are badly affected, eventually component degradation or failure occurs. Thermal management applications are used in order to dissipate generated heat and prevent problems that are originating from overheating of device.

Thermal management applications are divided into 2 categories:

1) Active thermal management
2) Passive thermal management

2.1.1.1 Active thermal management

Energy is introduced from an external source to enhance heat transfer in active thermal management systems. Rate of fluid in convection is increased by an external device hence heat removal rate increases. Disadvantageous properties of active thermal management are the need of electricity to operate and introduced noise to system while working. Active thermal management systems are also more complex and expensive passive thermal management systems. Forced air, forced liquid and solid state heat pumps are active thermal management types [5].

Forced air method

The most common active thermal management method is forced air. By forced air method heat flow rate is increased. In this method air is blown by a fan or compressor to fins, heat sinks, heat spreaders that were attached on the component or directly to heat generating component. Forced air cooling is more effective than convection.

Forced liquid method

Liquid flows through pipe in a closed loop system. When passing over the heated region or heat dissipater, liquid becomes hotter. Then hot liquid passes through the fins of the closed loop system, it gets colder since fins are open to air. Cooled liquid circulates repeatedly to continue cooling process. Forced liquid is more effective method than forced air method because liquids with higher conductivities than air can be circulated in pipes. Also it is more advantageous since system does not produce noise, however cost is higher and its design is more complex.

Solid state heat pumps

Solid state heat pumps are also known as thermoelectric coolers. For obtaining quick heat dissipation they are placed between heat source and heat dissipater. When voltage is applied to thermoelectric cooler, different temperatures are obtained between two sides of device and that enables conduction of heat. Even though solid state heat pumps have very long service life, they are not very efficient [6].

2.1.1.2 Passive thermal management

Passive thermal management methods rely on thermodynamics of conduction, convection and radiation. Passive methods are the most commonly used and easy implementation methods and also cost less than active thermal management methods. Heat sinks, heat spreaders, heat pipes, thermal interface materials are the passive thermal management solutions.

Heat sinks

Heat sinks are most widely used passive thermal management tools. It is a thermally conductive material that is attached on heat generating component. It has specifically designed shapes that increase heat release from electronic devices. Heat sinks have flat surface on one side and finned surface on other side. Flat surface is mounted on the heat generating component and the finned end is in touch with air. Finned surface is designed in its special shape to increase surface area. Heat is conducted through heat sinks to air, by convection of air heat is dissipated.

The most common area of usage of heat sinks is computers. In addition to the computers heat sinks are also used in cell phones, digital versatile disc players and also refrigerators. In order to supply to running the computers in desired speeds the heat generated needed to be transferred.

Working principle of heat sinks relies on the conductivity of the heat sink material. In the computers heat sink transfers the heat away from the central processing unit into the fins provides a large surface area for the for heat dissipation through the rest of the computer. Hence, both heat sink and processor are cooled. When the heat transferred to the heat sink from the heat generating component, a fan carries air across the heat sink and out of the computer. Additional fan which is installed above the heat sink cools the processors in most of the computers.

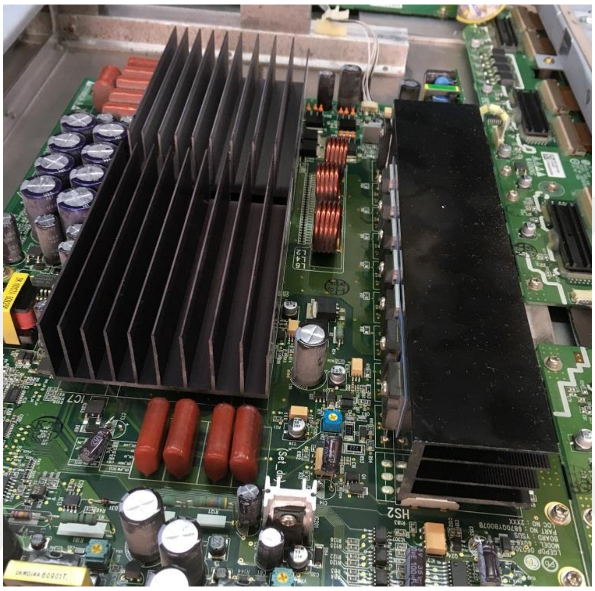

Figure 2.1 : Heat sink attached on a circuit board.

Not only in computers but also in transistors, voltage regulators, light emitting diodes, integrated circuits and power transistors thermal management is necessary. Also while soldering the electric circuit thermal management solutions are used.

When choosing a heat sink material the first thing to consider would be the thermal conductivity of the heat sink material. The higher thermal conductivity of a material is, the higher will be the efficiency of heat transfer. Also, the maximum will be the acceptable case temperature, the maximum power dissipation of the processor, the minimum thermal resistance, the maximum inlet temperature admittance to the heat sinks. The aim of the improvements of heat sinks includes finding lighter material of choice, more conductive materials. The heat sinks are not strictly required to be made of one type of material. There are designs of heat sinks also using the copper and aluminum which are the most commonly used heat sinks materials. However, the difficulty of this kind of design is that the poor bonding properties between these two materials.

Another important circumstance to consider about choosing the heat sink material is that the thermal expansion coefficients of the heat sink material and the heat source. The thermal expansion coefficient values of the heat sink and the heat generating component should have near values in order to provide a long life span to the thermal management [7].

Heat spreaders

Heat spreader is a metal foil or plate which has thermal conductivity. In order to spread the concentrated heat and divide among the heat to a larger area, heat spreaders are usually used as a thermal interface between the source of the heat and a secondary heat exchanger [8].

Heat pipes

Heat pipes comprises of a hollow close tube which contains a coolant or liquid. One end of the heat pipe is in contact with the heat source while the other end of heat pipe is in contact with the secondary heat source. Heat pipes are made of a thermally conductive metal that is flat or bended to complicated shapes therefore they are appropriate for limited space designs of boards. In the end which heat source is attached, the liquid is evaporating and travels to the cool end and condenses there. Since capillary action or gravity the condensed water turns back to the heat source attached end [9].

2.1.2 Heat transfer

When the temperature between different systems or interior of a system, heat transfer occurs. Between materials which are in thermal contact, from high temperature body to low temperature body heat flows. Heat is transferred in three ways, however engineering applications mostly uses the combination of these three different ways: Conduction, convection and radiation.

Heat transfer through a fixed wall that has hot face in one side and cold face at the other side occurs by heat conduction. Heat flow per hour is proportional to the temperature change through the stationary wall and wall area (A). Heat flow quantity is obtained by the equation. 2.1, if the thickness of the wall in the heat flow direction denoted by x and the temperature on a point on the wall is denoted by t:

$$Q = k.A.\left(-\frac{\Delta \mathrm{t}}{\Delta \mathrm{x}}\right) \tag{2.1}$$

Q denotes amount of heat transferred in Watts. Letter A denotes the area through that heat flows perpendicularly in square meters. k is the thermal conductivity and its unit is in W.m^{-1}.K^{-1}, while ΔT is temperature difference in Kelvin and $\Delta t/\Delta x$ is temperature gradient. Temperature gradient is negatively signed if temperature is higher at position x=X than the initial position where x equals 0. Generally conduction is related with solids but it is also applicable with some limitations in gases and liquids.

Heat is transferred by convection between hot and cold portions of fluids. When liquid is heated in a can, the liquid portions nearer to the bottom of the can becomes less dense due to the thermal expansion. The less dense liquid rises through the upper portions of liquid that are relatively colder and transfers heat by mixing as it goes up through colder portion. This is called free convection. If the mixing is done by stirring, agitation occurs and it is called forced convection. Convection is described as:

$$dQ = h.A.dt \qquad (2.2)$$

If the equation 2.2 is integrated Newton's law of cooling equation 2.3 is obtained:

$$Q = h.A.\Delta t \qquad (2.3)$$

Q here is amount of the transferred heat, h is heat transfer coefficient and ΔT is the temperature difference.

Radiant energy is transferred from high temperature is known as source to the low temperature known as receiver. Receiver absorbs part of energy when the energy is radiated by source and part of energy is reflected. Rate of heat transfer (2.4) by means of the given heat by source is formulated by Boltzmann based on the second law of thermodynamics and it is known as fourth power law.

$$dQ = \sigma.\varepsilon.dA.T^4 \qquad (2.4)$$

Thermal conductivity (k), heat transfer coefficient (h) and emissivity (ε) are values and that are determined experimentally. T is absolute temperature in Kelvin and σ is dimensional constant.

Fourth power of temperature difference is used for radiation, however in convection and conduction heat flow directly proportional to temperature difference [10].

2.1.3 Thermal conductivity

Thermal conductivity (k) is a specific property of materials. Units of thermal conductivity is watts per meter kelvin (W.m^{-1}.K^{-1}). Defines rate of heat flow per unit length in direction of flux and per unit temperature difference. Thermal conductivity is a prediction of the rate of energy loss through the material. Thermal conductivity of solids varies and materials which are good conductors of heat have high k values and they are conductors. Materials which are weak conductors of heat are insulators.

Thermal conductivity is affected by production method, present impurities and inclusions. Also as exterior factors, it is dependent on temperature and pressure. For most materials conductivity does not change much with medium temperature change.

2.1.3.1 Thermal conductivity of metals

In metals valance band is not completely filled and there are free electrons which have ability to move with a little thermal excitation. Electrons play an important role for thermal conduction. Phonons have very little attribution for thermal conductivity of metals. Pure metals have higher thermal conductivity than alloyed metals since there are no impurities present to scatter or decrease the motion of electrons.

Temperature change causes thermal conductivity to decrease or increase. Increased or decreased thermal conductivity with increased temperature arises from two competing factors. When temperature increases, increased lattice vibration and increased energy of electrons causes thermal conductivity to increase. Energy of electrons increases, more carriers created and increased lattice vibrations obtained due to higher temperature. However there may be a decreased thermal conductivity because lattice vibrations scatter electrons and reduces mobility of electrons.

Table 2.1 : Thermal properties of various metals under standard conditions

Metal	k ($W.m^{-1}.K^{-1}$)	α ($10^{-6}.K^{-1}$)
Silver	428	19.7
Copper	398	17
Gold	315	14.2
Aluminum	247	23.6
Tungsten	178	4.5
Brass (Cu70Zn30)	120	20
Nickel	90	13.3
Iron	80	11.8

Thermal conductivity in metals also depends on crystal structure defects, microstructure, and processing. Thus, cold-worked metals, solid-solution-strengthened metals, and two-phase alloys might display lower conductivities compared with their defect-free counterparts.

2.1.3.2 Thermal conductivity of ceramics

In ceramics there are no free electrons. Therefore ceramics are not commonly known as good conductors of heat. Heat is conducted by lattice vibrations which is called phonons. Since phonons are not effective heat energy transporters ceramics are used as insulators. Porosity in ceramic materials decreases thermal conductivity because porosities are air bubbles trapped in material and air has thermal conductivity of 0.02 $W.m^{-1}.K^{-1}$. Amorphous ceramics has even lower conductivities because more phonon scattering occurs when the structure is not ordered and regular. Although it is unusual that a non-metallic material to have high thermal conductivity, thanks to its extremely rigid crystal structure diamond conducts heat effectively by phonons. Single crystal diamond has a thermal conductivity higher than 2400 $W.m^{-1}.K^{-1}$ around room temperature when it is in its purest form. ^{12}C which is isotopically enriched polycrystalline form of diamond has thermal conductivity of 3300 $W.m^{-1}.K^{-1}$. Among all known materials diamond has the highest thermal conductivity [11].

Being a non-metallic material and insulating electricity is an advantageous property of diamond to be part of thermal management applications in electronics.

Table 2.2 : Thermal properties of various ceramic materials at SC.

Ceramic	k ($W.m^{-1}.K^{-1}$)	α ($10^{-6}.K^{-1}$)
Synthetic Diamond	1000-2200	1.1
SiC	280-400	3.8
AlN	285	4.3
MgO	37.7	13.5
Al_2O_3	39	7.6
Spinel	15	7.6
Soda lime glass	1.7	9
Fused silica	1.4	0.4

2.1.3.3 Thermal conductivity of polymers

Thermal conductivity of polymers depends on its crystallinity degree. When polymers becomes more crystalline conductivity increases. Energy is transferred by molecular vibration or rotation of chains. In ordered structures vibrations and rotations becomes more effective and coordinated so thermal conductivity increases. Thermal conductivity value of polymers is around 0.3 W/m^{-1}.K^{-1} therefore they are used as heat insulators.

2.1.4 Thermal expansion

Thermal expansion is a physical property of materials. It is a known fact that solid materials expand when they exposed to heat and when cooled down they shrink. This dimensional change that is originated from the temperature change differs from a material to another. For solids the change in length expressed by the equation 2.5.

$$\frac{l_f - l_0}{l_0} = \alpha(T_f - T_0) \tag{2.5}$$

When temperature changes from T_o to T_f, length of material changes itself from l_o to l_f. α denotes here the CTE in unit of K^{-1}. Other than linear calculations, CTE can be calculated by volume change. However, since all materials do not show isotropic properties linear coefficient is rather preferred than volume coefficient. For isotropic materials the volume CTE is 3 times of linear CTE. Thermal expansion is the phenomena of dimensional increase of a material with temperature raise under constant pressure. It is a physical property of materials and different materials show different amounts of elongations.

2.1.4.1 Material selection for thermal management applications

For a material to be used in thermal management applications it needs to have certain properties. It is a crucial decision to choose a material that meets the expectations. Having high thermal conductivity is the most important aspect in selection of heat sink material, however CTE should also be taken into consideration. A material that conducts heat effectively but has a CTE value that is incompatible to that device on which heat sink is attached will not work efficiently therefore may cause problems that arise from the overheating of the device. When CTE of recently used heat sink materials are compared to that of semiconductor device it can be foreseen that abovementioned issue is inevitable (Figure 2.2). On the ground that the CTE mismatch, heat sink and semiconductor materials elongate and shrink in different amounts. Therefore this couple have a tendency to bend when temperature arises and later on their contact will become damaged owing to repeated heating and cooling.

When producing a material to be used in thermal management applications, the desired combination of properties are high thermal conductivity and a CTE value matching with the part to which the heat exchanger material will be attached. Metals are good conductors of heat but their usage in thermal management is disadvantageous since they show high dilatation [3].

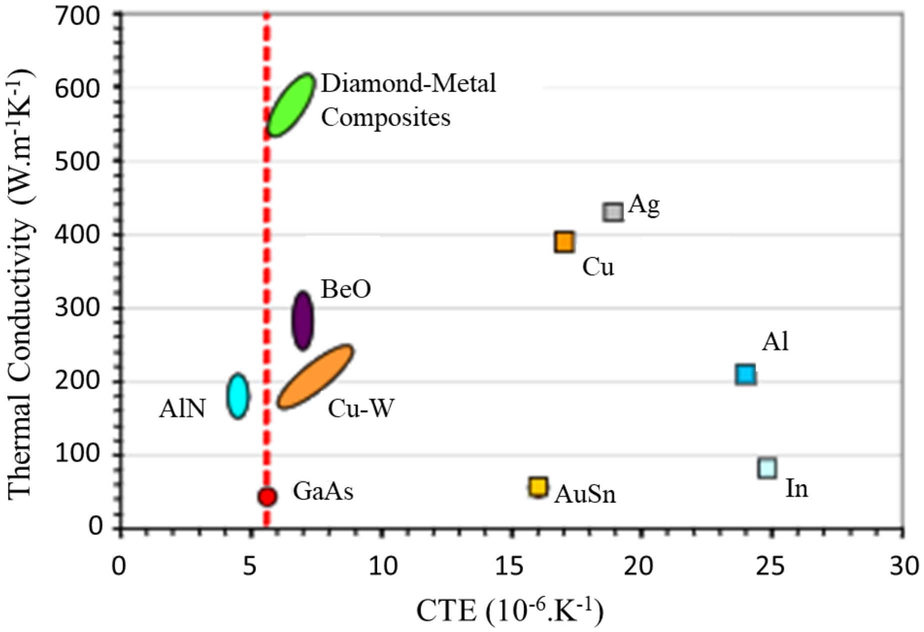

Figure 2.2 : Thermal conductivity and CTE values of certain materials [12].

According to Schleuning et al., by producing copper-tungsten alloys, problem arising from the CTE mismatch is overcome. However as it can be seen from the Figure 2.2, thermal conductivity of copper decreases when it is alloyed with W [12]. Hence, one should come up with a solution both reducing CTE and not sacrificing value of thermal conductivity. One way to do so is producing composite. Since diamond has supreme thermal conductivity and CTE that is compatible with that of semiconductor device, it is an outstanding material to be in use as a reinforcement in MMCs that are produced for thermal management applications. Studies show that improved thermal conductivity along with suitable CTE are obtained by production of copper-diamond composite by processes that require high temperature and high pressure [13-19].

2.2 Composite Materials

Composite materials are made by joining two or more materials together, which often demonstrate different properties than each other. Thanks to composite materials, desired properties are achieved by bringing various combinations together. Composites are selected to attain unusual combinations of strength, stiffness, density, hardness, corrosion resistance, high temperature properties, conductivity, or wear resistance [4]. Classification of composite materials can be made by either based on the matrix material or based on the reinforcement. Based on the matrix material composite materials are classified as metal matrix composites (MMC), ceramic matrix composites and polymer matrix composites. Composite materials are also classified as fiber-reinforcement composites, particulate composites and structural composites based on reinforcement. Composite materials according to reinforcing phase is classified as fiber reinforced composites, structural composites and particle reinforced composites [20]. Fiber reinforced composites are divided as continuous and aligned, discontinuous and aligned and discontinuous and random. Fiber reinforced composites have properties that differ directionally in case of unidirectional alignment of fibers. Structural composites are classified as laminates and sandwich panels. Laminar composites comprises of multiple layers of reinforcement material that are held together by matrix material. The direction of each layer differs from other layers. Laminate composite materials show anisotropic properties. When structural composites are produced by placing a honeycomb structure between two face sheets that are attached to honeycomb core with an adhesive layer, sandwich panels are obtained. In particle reinforced composites, reinforced phase is distributed in the matrix phase in such geometrical shapes as spherical, ellipsoidal or irregular shaped particles. The geometry of particles may differ but dimensions required to have approximately same values in all directions in order to evaluate reinforcement as particle. Isotropic properties are achieved by even distribution of particles in matrix phase. When reinforcement particles are larger than 0.1 μm, composite is classified as large particle reinforced composite. With particles smaller then that value, composite is named as dispersion strengthened composite and this formation brings along alike consequences as in dispersion strengthening in alloys [21].

Composite materials are classified as ceramic matrix composites, polymer matrix composites and metal matrix composites based on class of matrix material. Matrix material specifies method of production, mechanical behaviors and function of composite materials. Production conditions also specify which materials can be chosen as reinforcement since reinforcement material should not undergo chemical reactions or physical changes at production temperatures. MMC materials are divided into two: first group comprises of metals and alloys and second group comprises of intermetallic matrixes. Without considering type of matrix material, interface is very important for controlling properties. Well defined interfaces separate matrix and reinforcement phases. Strength of interfacial bonding is important for overall behavior of properties. Higher bond strengths are achieved by use of coupling agents or mechanical interlocking.

2.3 Production Methods of MMCs

MMC production methods can be classified as liquid state methods, solid state methods and deposition techniques [20].

2.3.1 Liquid state production methods

Liquid state production process is conducted by various methods where matrix material is in the liquid phase. This includes stir casting and infiltration methods.

2.3.1.1 Stir casting

Stir casting, is a production method of composite materials, involves dispersion of reinforcement particles in molten metal matrix, casting and solidification. Reinforcement phase is dispersed in matrix by mechanical stirring. Matrix metal is melted in a crucible. Melt is stirred by stirrer and reinforcement particles are added to the molten metal for dispersion of particles. Stirring is very important to prevent particles from settling down. Stir casting method is an economical method, especially when big parts are produced a decrease of very large amounts of the production cost is observed. Although being the most economical liquid state metal matrix composite production method, stir casting has drawbacks that cannot be disregarded. To start with, attainable volume percentage of dispersed phase is less than 30 vol %. Wetting problems between matrix and reinforcement phase is an important concern in this method as in all the liquid state production methods. Uniform distribution of dispersed phase is very difficult to obtain by stir casting method. Reactions between matrix and reinforcement as well as reactions with atmosphere may occur and may cause negative effects on base material. In order to prevent those reactions degassing process should be applied to the melt before introducing reinforcement to molten matrix metal. Since stir casting involves casting of melt, common solidification problems such as shrinkage and porosity may be present in the product. Therefore solidification stage should be practiced carefully [22].

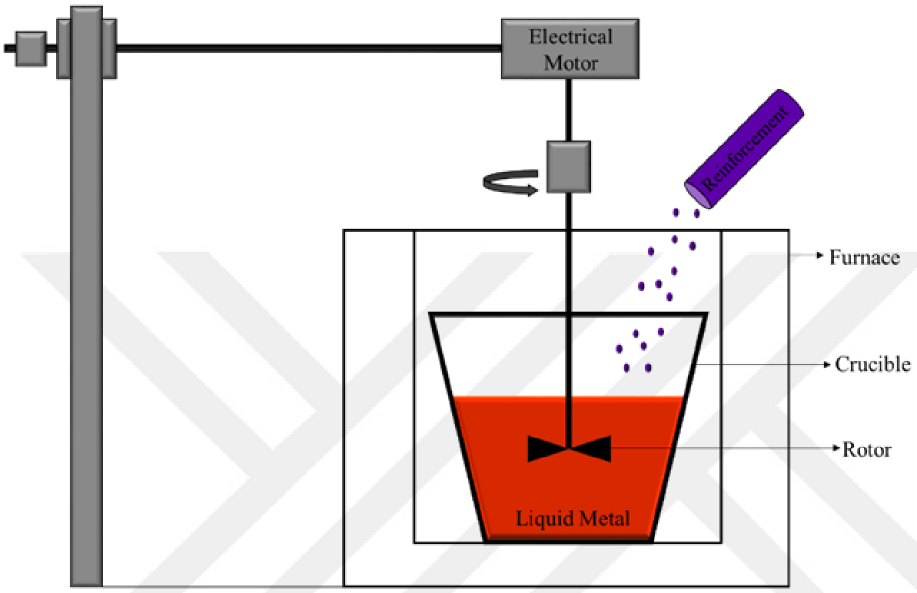

Figure 2.3 : Stir casting process illustration [23].

2.3.1.2 Infiltration method

Infiltration technique is the method of choice when high volumetric concentrations of ceramic reinforcement phase is desired in MMC composite. Infiltration process is simply accomplished by penetrating molten metal into porous preformed ceramic structure. Preformed structure can be in fiber, woven, and particle forms. Porosities are eliminated since molten metal fills present gaps in preformed base material. Additionally infiltration process is advantageous since volume concentration and distribution of reinforcing phase is well managed [24].

Main concern is, as in all other liquid state composite production methods, in infiltration method molten metal should wet the ceramic body. Liquid metal may need to be heated to a temperature that is higher than its melting point to ease its filtration into structure.

Infiltration process can be examined under two headings: spontaneous infiltration and forced infiltration. Spontaneous means it does not require any external force for infiltration. It is economically more beneficial than other infiltration methods, it requires a cheaper and less complex setup and is more practical to perform. However when there is not enough wetting between matrix and reinforcement phases an external force is required (forced infiltration). Otherwise the interface between matrix and reinforcing phase will be weak and it will dramatically affect the material property depending on the application area. If the material will be under mechanical stress it will fracture earlier, if the material will be used in thermal management applications, it will not have the desired thermal conductivity nor the appropriate expansion coefficient and due to the weak thermal interfaces material will conduct heat poorly while it will expand at higher values. Infiltration techniques differ from each other based on which technique is used to force molten metal into preformed structure [25,26]. Forced infiltration techniques are; gas pressure infiltration, pressure die infiltration, centrifugal infiltration, vacuum infiltration, Lorentz force infiltration, ultrasonic infiltration and squeeze infiltration.

In pressure assisted liquid metal infiltration, infiltration is executed under vacuum condition in an autoclave. Melt is forced through preformed reinforcement structure by pressurized gas. In gas pressure infiltration pressurized gas is used for penetration into preform. Usually operates with vacuuming from the other end of the chamber to throw air out to expel trapped air in porous body. Main disadvantage cost increment due to inert gas usage as pressurized gas.

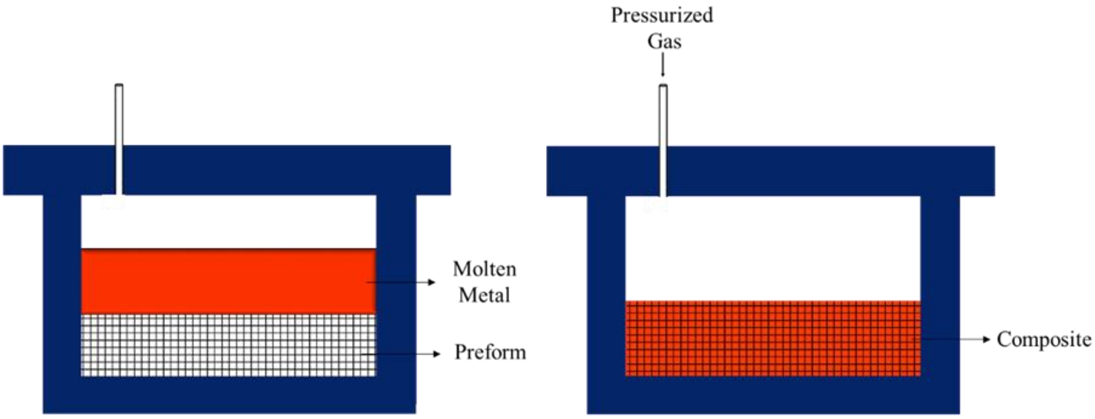

Figure 2.4 : Illustration of Gas Pressure Infiltration (GPI) Technique [27].

Pressure die infiltration method uses a plunger to ease molten metal infiltration into preform in a rigid die. Uses technology of die casting in which plunger moves horizontally. It is a low cost method, however preform may be deformed due to compressive force. Therefore compression pressure should be preferred as not too high to protect preform but high enough to ease infiltration of metal.

In centrifugal method, porous preform is in a mold and rotational forces acting on forces molten metal to penetrate. In vacuum infiltration, negative pressure is applied to the preformed ceramic structure. Blanks in preform becomes evacuated and metal penetrates into the structure.

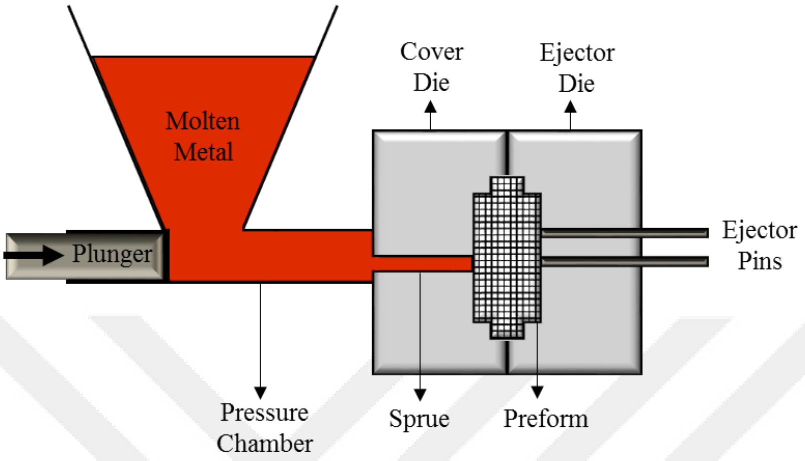
Molten
Metal
Cover
Die
Ejector
Die
Plunger
Ejector
Pins
Pressure
Chamber
Sprue
Preform

Figure 2.5 : Illustration of Pressure Die Infiltration (PDI) technique [28].

Squeeze infiltration is one of the most widely used infiltration method. It is a near net shape production method for MMC. In squeeze casting method preformed structure and molten metal are placed in a die. Plunger applies pressure and forces molten metal to infiltrate. This method uses squeeze casting technology in which plunger moves vertically. Squeeze casting uses pressures in the range of 50-100 MPa. As it applies for pressure die infiltration method, high pressure may deform the preform.

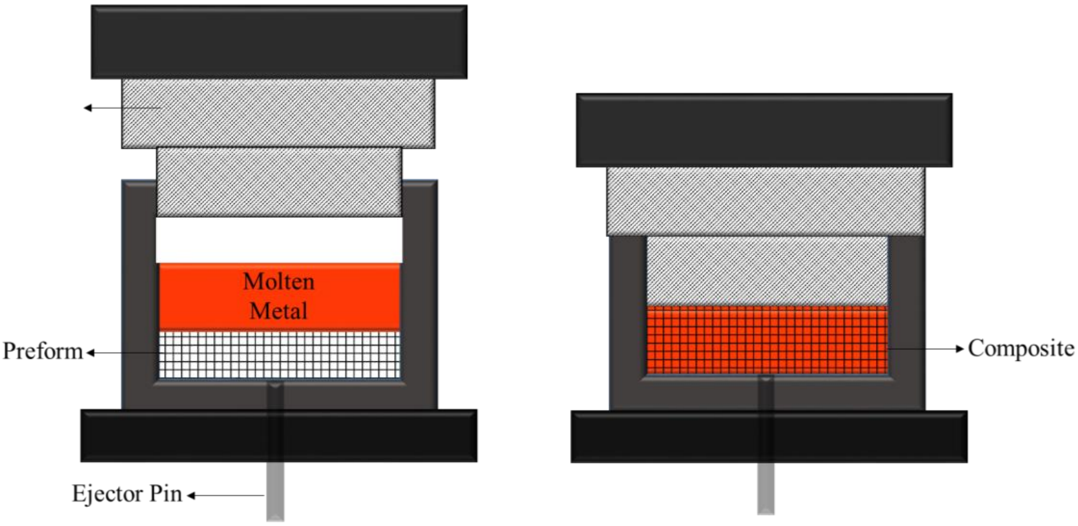
Molten
Metal
Preform
Ejector Pin
Composite

Figure 2.6 : Illustration of Squeeze Casting Infiltration technique [27].

Lorentz force infiltration is a new technique which uses electromagnetic forces. Preform is immersed in melt and high frequency magnetic pulse is applied to melt. Lorentz forces are obtained for high speed penetration of molten metal.

Ultrasonic infiltration method uses pressure waves generated by ultrasonic vibration. A transducer is used for driving force for metal infiltration through ceramic structure. By movement of ultrasonic waves to molten metal through a horn some bubbles form. With the collapse of the bubble, shock wave arises near to molten metal and supports infiltration [29].

2.3.2 Solid state production methods

Solid state MMC production methods rely on diffusion between reinforcing and matrix phases. High temperatures and pressure is required for processes. Solid state methods include powder metallurgy and diffusion bonding.
Powder metallurgy method is used when discontinuous reinforcement phase is desired. If reinforcement phase is desired to be continuous diffusion bonding method is the method of choice.

2.3.2.1 Powder metallurgy

Powder Metallurgy is a process for fabricating components by compacting finely powdered metallic or non-metallic or both materials. Production of composite materials by powder metallurgy method initially requires pulverization of the raw materials. Blending of powders, compaction and sintering are three steps of production by powder metallurgy. Advantage of powder metallurgy method is net shape or near net shape production. However, the interface between matrix and reinforcement is a significant issue to consider. In MMC production by powder metallurgical method, reinforcing material should have good wettability by metal matrix for a reliable interface. If reinforcing material has poor wettability with matrix material, powders should be coated by a secondary material to improve properties of overall composite material by eliminating interfacial problems.

Blending stage includes mechanical mixing of raw material powders of both reinforcement and matrix material. Reason for blending is to obtain homogeneous mixture. For avoiding porosity in end product, powders with different particle sizes are required to be blended. Some additives should also be added in order to prevent undesired problems while production. Lubricants may be needed for reduced friction between particles and in order to inhibit adhesion between die wall and particles during compaction step. Flocculants are also added to prevent agglomeration of powders.

In compaction stage blended powders are placed in a die or a mold and high pressure is applied by hydraulic press or mechanical press to compress powders and obtain green compact. Green compact has enough strength and it can be handled. After compaction green compact is removed from the die for sintering stage. Sintering requires temperatures around half of the melting temperature of material. At the stage of sintering green compact is heated to sintering temperature. While particles bond to each other, pores are eliminated. Sintering time should be considered carefully. If sintering duration at sintering temperature is long, grain growth occurs. Grain growth effects mechanical properties negatively.

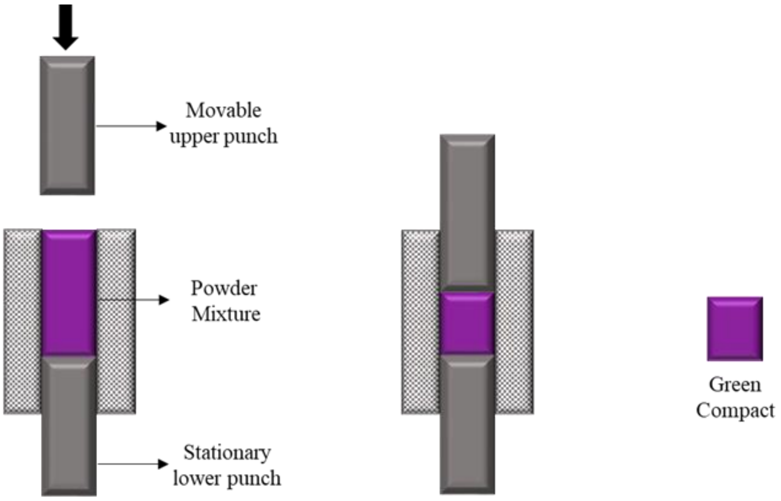

Figure 2.7 : Compaction stage of powder mixture.

2.3.2.2 Sinter forging

Initially, reinforcement and matrix powders are mixed. Cold compaction, sintering and forging processes applied. Nearly full density is obtained by sinter forging method. It is a near net shape production method.

2.3.2.3 Diffusion bonding

At elevated temperatures atomically clean solid surfaces are joined together by inter-diffusion of atoms. Matrix is present as foils, and reinforcement particles are in fiber form. Elevated temperatures are required for diffusion bonding. Laminated and multilayered composites are produced by this method.

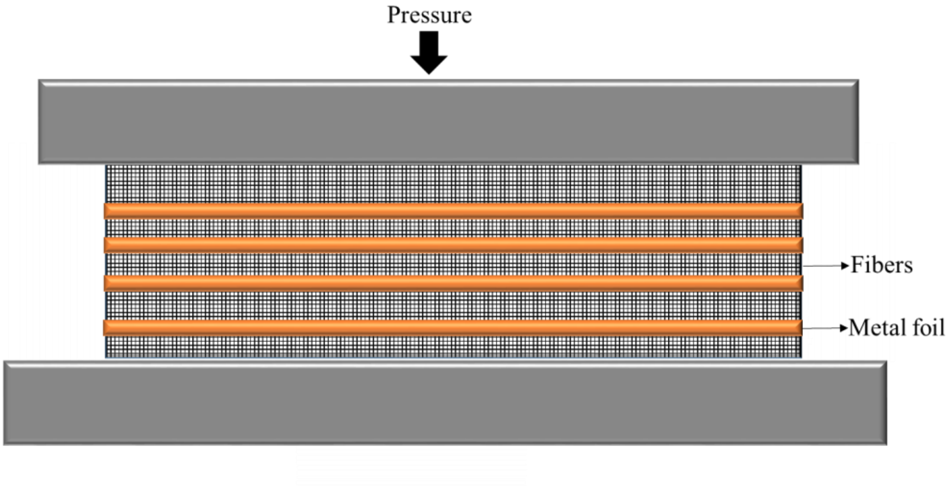
Pressure
Fibers
Metal foil

Figure 2.8 : Illustration of diffusion bonding method.

Fiber orientation and fraction of reinforcing phase is controlled. Required temperature is about 50%-90% of absolute melting temperature of main material. Pressure is applied in this process. Pressure application time ranges from minutes to hours. Diffusion bonding is a metal-metal composite production method.

2.3.3 Spray deposition

Spray deposition technique relies on spraying molten metal onto fibers or particles of reinforcement material to create a monotape. Reinforcing fibers or particles are winded on a drum which is foil coated, molten metal sprayed onto them.

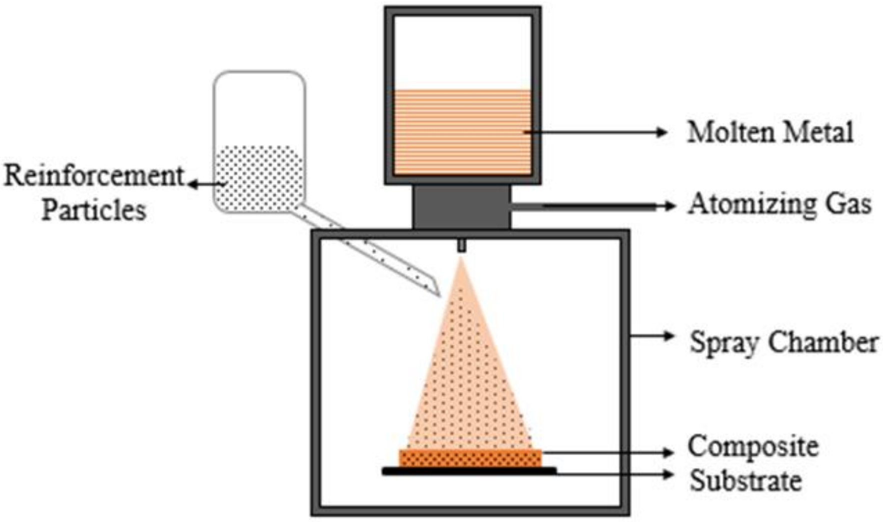
Molten Metal
Atomizing Gas
Reinforcement Particles
Spray Chamber
Composite
Substrate

Figure 2.9 : Illustration of spray deposition technique [27].

Spray deposition includes a spray gun for atomization of molten metal, while heated reinforcing particles are being added into structure.

2.3.4 Electrochemical composite fabrication

Pure metals, ceramics or polymers can be incorporated in metal deposit. Combination of range of these materials, variety of composite materials can be produced by electrochemical method. Conventional MMC production techniques which are mentioned earlier are disadvantageous because these techniques require to be practiced at high temperatures and also necessitates complex and expensive equipment. Electrochemical method is operated at temperatures around room temperature, also does not require complex equipment. Moreover in conventional techniques, wetting is very serious problem which causes weak bonding between matrix and reinforcement phases. Solid-liquid interactions is interpreted by wetting phenomenon. Wetting could be liquid spreading over a solid surface, displacement of one liquid with another liquid, or penetration of a liquid into porous structures. Surface characteristics of a liquid can be quantified by measuring contact angle of liquid droplet on a solid surface. Contact angle is the angle between solid liquid interface and liquid vapor interface. Depending on contact angle between solid and liquid, it comes to light whether it is a wetting liquid or non-wetting liquid. When angle of contact is higher than 90° droplet forms and non-wetting situation occurs. When angle of contact is lower than 90° liquid spreads over surface and wetting occurs. For a liquid to penetrate effectively, contact angle should be very small. Zero contact angle stands for complete wetting. When contact angle is higher than 90^{o} infiltration is inhibited since no wetting occurs. As it appears in conventional production of copper diamond composites, diamond cannot be wetted by copper. Weak interfacial bonding between copper and diamond results in high thermal resistance. Therefore conductivity decreases. At 1673 K the contact angle between copper and diamond is calculated as 128.7° [30].

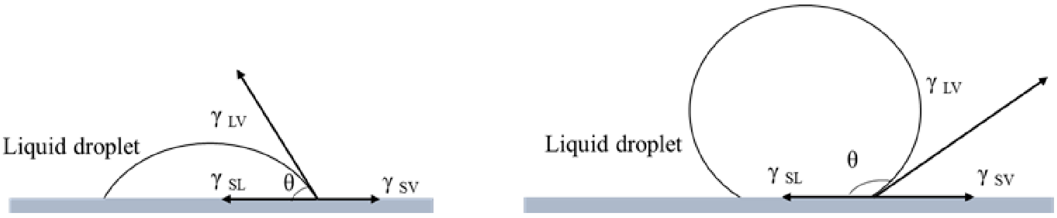

Figure 2.10 : Wettability of a liquid, wetting angle smaller than 90° (left), larger than 90° (right).

T. Young described contact angle at three phase boundary by equation;

$$\gamma_{SV} = \gamma_{SL} + \gamma_{SV} . cos\theta \tag{2.6}$$

γ_{SV} indicates interfacial tension between solid and vapor, γ_{LV} indicates interfacial tension between liquid and vapor, γ_{SL} indicates interfacial tension between solid and liquid and θ is equilibrium contact angle [31].

When no wetting occurs between diamond particles and copper matrix, interface effects thermal properties of composite material in an undesired way. A loose interfacial bonding between matrix and reinforcement results in collapse as a result of thermal cycling. In order to overcome wetting problem, one solution is to modify the particle surface characteristics of the reinforcement by changing surface chemistry or forming another layer for obtaining improved wettability [32]. Addition of carbide forming agents serves to purpose of enabled wetting between copper matrix and diamond particles [33-40]. Formation of alloyed matrix is another solution to overcome interfacial problem [14,18,41,42].

Electrochemical production of composite materials does not include melting process therefore wetting problem is overcome. Electrochemical composite production is succeed based on the principle that co-deposition of insoluble particles in the electrolyte within metal deposit. Therefore electrolytic deposition principles and practice should have been investigated essentially. Electrodeposition is the process in which electrical current is used for metal deposition on a substrate.

An electrodeposition system includes electrolyte, anodic half reaction, cathodic half reaction and electronic contact. Anode and cathode electrodes are immersed in an electrolyte and DC current is applied to electrodes, thus the electronic circuit is completed and process begins. Electrolyte is an aqueous solutions of salts therefore it contains positively charged ions which are known as cations and also negatively charged ions which are named as anions. Anode and cathode electrodes are immersed in an electrolyte and DC current is applied to electrodes, thus the electronic circuit is completed and process begins. Electrolyte is an aqueous solutions of salts therefore it contains positively charged ions which are known as cations and also negatively charged ions which are named as anions. Figure 2.11 represents a basic electrolysis system, consisting of an anode, a cathode both connected to a power supply and both immersed in an electrolyte. Cathode and anode are electrically conductive solid materials and both are named as electrodes. Reduction of metal ions from solution takes place on the cathode surface while by anode surface overall charge neutrality is provided. Anode material can also have a second function of providing metal ions to the solution.

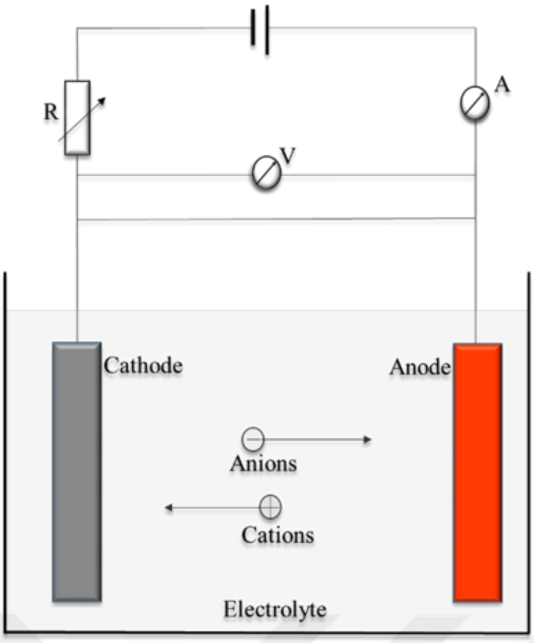

Figure 2.11 : DC electrolysis system.

Anodic and cathodic half reactions can respectively be given as:

$$Me^0 \rightarrow Me^{z+} + z.e^- \tag{2.7}$$

$$Me^{z+} + z.e^- \rightarrow Me^0 \tag{2.8}$$

There are two types of anodes which are known as soluble anodes and permanent anodes. Soluble anodes are the ones supplying to solution the same type of metal ions that are deposited on cathode surface. For instance in copper electrodeposition copper anodes are soluble anodes and this type of anodes diminishes as reaction proceeds. The second type of anodes is permanent anodes, for example titanium anodes coated with platinum are permanent anodes. When these type of anodes are used, metal ions should be supplied to solution in the form of metal salts and anodic reaction is now:

$$H_2O \rightarrow 2H^+ + \frac{1}{2}O_2 \uparrow + 2e^- \tag{2.9}$$

Under definite conditions a dissolution of a metal is observed when it is submerged in the electrolyte. Metal atoms that were located in lattice leave their position and form cations released through electrolyte. As a subsequent metal now has a negative charge and electrostatically attracts positively charged cations to itself. This dynamic equilibrium is shown by:

$$Me \leftrightharpoons Me^{+z} + z.e^- \tag{2.10}$$

If no net reaction observed it is said to be under equilibrium. That means forward and reverse reactions occur in same rate.

$$i_c = i_a = i^0 \tag{2.11}$$

i_c, i_a, i^0 indicates cathodic current density, anodic current density and exchange current density respectively.

However when electrical current is applied to the system, there is no more equilibrium between anodic and cathodic reactions and reaction is said to be tilted and this can be either forwards or backwards. Charge negativity of metal strengthens when it is connected to electron source and more positively charged cations are attracted by metal in that case metal is cathodic. Under this circumstances deposition occurs. For anodic dissolution to take place, metal should be attached to positive end. Positively charged metal repulses cations and anodically dissolves. With an increase in voltage, the rate of reaction is forwards or reaction reverse increased and a net reaction is observed due to overpotential (η). Overpotential is indicated as:

$$\eta = |\varepsilon - \varepsilon_{Me/Me^{+2}}| \tag{2.12}$$

Overpotential can be anodic or cathodic. Anodic overpotential drives equation in anodic direction and cathodic overpotential drives equation in cathodic direction. If it is assumed that the only rate determining step in cathodic process is charge transfer across electrical double layer overpotential is defined as activation overpotential. (η_D) Activation overpotential defines the energy need to overcome activation energy of reaction. Rate of reaction increases with increasing overpotential. Activation overpotential is important in the redox reactions which has low exchange current density, i^0. When exchange current density is high, reaction becomes more reversible and activation energy barrier is lowered. Rates of anodic and cathodic reactions are given by the formulas:

$$i_a = i^0 . e^{(\alpha . z . F/RT)\eta_D} \tag{2.13}$$

$$i_c = -i^0 . e^{-[(1-\alpha).z.F/RT]\eta_D} \tag{2.14}$$

α is transfer coefficient and its value lies between 0 and 1, however mostly it has a value of 0.5 and it stands for charge transfer in forward direction. Based on this $1 - \alpha$ stands for the dependence to potential in reverse direction. R denotes gas costant in $J.mol^{-1}.K^{-1}$ and absolute temperature denoted by T in Kelvin. On the basis of a given current density, one calculates activation overvoltage as following:

$$\eta_D = \frac{RT}{(1-\alpha.z.F)} \cdot \ln\left(\frac{i^0}{i_c}\right) \tag{2.15}$$

This formula implies that when exchange current density decrease, overvoltage increases [43].

When voltage is applied to system electron flow occurs. Anode metal dissolves anodically and cations are released. Then cations migrate through cathode and anions from solution move through anode. Flow of current by movement of charged particles is known as ionic electrolytic conductance or ionic current. Migration, diffusion and convection are the three main mechanisms of ion delivery. Migration is the movement of charged particles under potential gradient. Potential gradient is found by dividing voltage to distance between electrodes. Rate of ion movement in solution is determined by magnitude of potential gradient. Anions are attracted to the anode and cations are attracted to the cathode. Collisions with molecules of solvents, viscous drags, hydration sheets of ions hinder the ions. Therefore ions have very low velocity so that migration contribution to overall ion procurance is neglected.

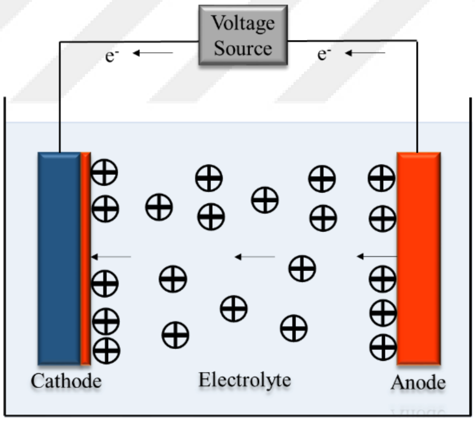

Figure 2.12 : Movement of ions through the electrolyte.

Convection is reactant movement with electrolyte. Movement of bulk of solution by stirring, air agitation or pumping causes diffusion layer to be thinner. Thinner diffusion layer is beneficial for diffusion.

In bulk solution concentration is assumed to be same with electrode surfaces. When current flows, there is a concentration gradient formation since reaction at electrode surface removes species. The movement of species from high concentration regions to regions of low concentration resulted from removal of species is driving force for diffusion. Diffusion layer is also known as Nernst layer and thickness of Nernst layer is approximately 0.2 mm, by forced convection it can decrease to 0.001 mm. Only transport mechanism within the Nernst diffusion layer is diffusion.

If concentration on the Nernst layer is zero, it means that species are reduced immediately when they arrive to electrode surface and in this case the current is said to become diffusion limited current density or mass transport limited current density. At this point, if voltage is increased, no current increase occurs. At the maximum current density values that metal can be deposited, powdered or crumbling deposit forms. From the relation of current density with potential, shown in Fig. 2.11, it is observed that area 1 is activation controlled, 2 is intermediate region with both mechanisms rate determining, 3 is under diffusion controlled. Transport of ions from solution through surface of cathode occurs by convection and diffusion. In electrical double layer which is formed at interface between metal and solution, ad ions discharge to form so called ad atoms.

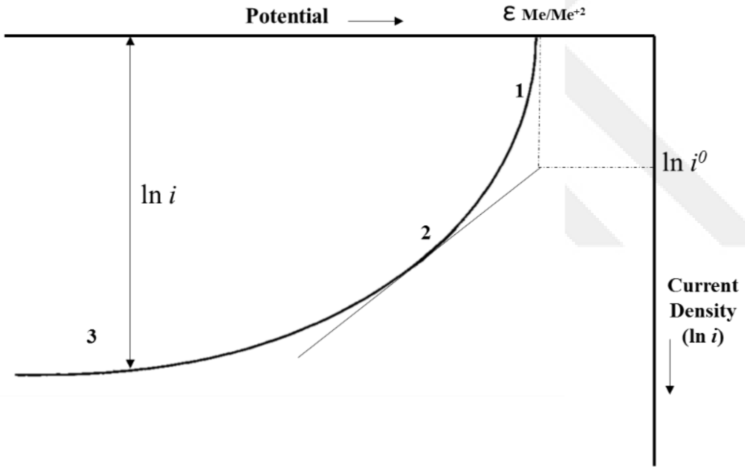

Figure 2.13 : Relation of current density with potential.

Hydrated metal ion transports to the cathode from bulk solution. Strips the hydration sheath at the interface between metal and solution. Transfers its charge at cathode surface by forming adsorbed atom (ad-atom). Crystal nuclei is formed by diffusion of adsorbed atom at the surface. Adsorbed atoms join together to form metallic layer.

As it applies for every electrodeposition processes, copper electrodeposition includes a cathode, an anode, an electronic contact between the electrodes and the appropriate choose of electrolyte.

Anodes in copper electrodeposition can either be sacrificial copper anodes or insoluble anodes. However it is more practical to use sacrificial copper anodes, since by usage of sacrificial anodes copper ion concentration in the bath is kept constant. By using insoluble anodes thick deposit cannot be formed since electrolyte will deprived of copper ions before the desired thickness is achieved. With sacrificial anodes ions are continuously supplied. For these reasons it is more practical to use sacrificial anodes in electrodeposition of copper. Cathode material can be either copper or other materials such as iron, graphite, nickel.

For copper electrodeposition alkaline cyanide and pyrophosphate complex ion, acid sulfate and fluoborate simple ion systems are used. Other types are not satisfying the expectations of deposit characteristics or being stable. The most common type electrolyte for copper deposition is acid copper sulfate solution. When thick layer of coating is desired, cyanide solutions are not favorable. Cyanide solutions are generally used when thin layers of copper coating is desired, for instance intermediate layer before coating with Al, Be, Zn metals. Another issue is cyanide solutions are toxic and wastes from cyanide solutions requires careful treatments. Pyrophosphate solutions are lack of high throwing power. Fluoborate solutions are convenient solutions since at high current densities copper deposition can be done. However the same duty of fluoborate solutions is met by sulfate solutions with easier control and lower cost. By electrodeposition, metals can be plated on a substrate. Moreover, metallic components which have complex shapes are produced by electroforming method. By electroforming very complex shaped materials can be produced. Materials for which high precision is so important, have no alternative production method other than electroforming method. It is not just small components that one can produce by electroforming. As well as very small pieces, one can also produce very large components for automotive or aerospace industry by electroforming method. Electroforming is very similar to electrodeposition in regard to equipment and operation. Specialty of this method lies in the usage of a cathode that possesses the negative shape of desired product. This specially shaped cathode is named as mandrel. Electrodeposition continues until the deposit reaches the thickness levels so thick so that the deposit remains its shape even after the removal from mandrel. To achieve exact repro of model, throwing power of electrolyte has to be very high because metal should be properly deposited on all over the surface.

When insoluble particles exists in the electrolyte, these particles have a tendency to codeposit with the metal ions. Formerly insoluble particles are thought to be impurities that are desired to be eliminated. However afterwards it became evident that these particles have remarkable effects on deposit properties. Herewith deposition of composite coatings by electrodeposition is succeeded by addition of insoluble particles in electrolyte.

2.3.5 History of composite electrodeposition

In order to produce a composite deposition, experimental system is designed as it is designed in conventional electrodeposition processes. After the system is set insoluble particles, that later on constitutes reinforcement phase of composite material, are added to the electrolyte. Particles need to be kept suspended on the area between anode and cathode surface during deposition. When metallic phase deposits, the insoluble particles are trapped in growing metals matrix. Numerous models were developed to explain how entrapment of insoluble particles into the deposit occurs. Although there were traces of composite electrodeposition applications at the beginning of 1930's, scientifically, co-deposition of inert particles from electrolyte into the metal deposit started in sixties. In 1964, Williams and Martin proposed that agitated particles in electrolyte are trapped at cathode surface while metal layer is growing [44]. However a study of Brandes and Goldthorpe rejected their idea. They thought that the mechanical entrapment cannot be the only reason of particle codeposition and there should be some attractive forces which hold particles at surface of the cathode. Experimental results were also promoting their idea in 1967. According to Bazzard and Boden some residence time on surface of cathode was needed for particles to incorporate in the metal layer. Empirical and more convenient models develop after the first attempts. Guglielmi explained a two-step phenomena which is accepted as a significant step for understanding composite deposition with regard to electrode and particle interaction. Firstly, particle that comes to surface of the cathode is loosely adsorbed there. Loosely adsorbed particle still has ionic cloud when it is adsorbed on cathode surface. In the second step ionic cloud is lost and particle becomes strongly adsorbed [45]. Kariapper and Foster stated that there are two roles of adsorbed metal ion. Firstly, positively charged metal ion is attracted to negatively charged cathode electrode electrically. Secondly, when positively charged metal ion is reduced at cathode surface, particle and cathode bonds physically.

In 1987 Celis et al. offered improvement of Guglielmi's model. Model comprises of 5 steps [46];

I. Ionic cloud formation due to ion adsorption
II. Transportation of particles through cathode surface by convective diffusion

III. Adsorption of particles with their ionic cloud on the cathode surface
IV. Shedding of ionic cloud
V. Particles included in growing metal deposit

According to Celis et al. Guglielmi’s model was inadequate for explaining the relationship between particle content in deposit and current density and they described particle amount in deposit at a given current density by using probability. Mass transport of ions that are being transported to working electrode are proportional to each other. Volume fraction of particles in deposit increases when deposition is charge transfer controlled, decreases when deposition is mass transport controlled. Relying on experiments that were conducted with Cu-Al_2O_3, Au-Al_2O_3, model was in a good agreement with experimental results. However according to Degrez and Winand (1984) there were questionable issues since there was a mechanism change in copper reduction mechanism observed. This change was not relying on the change in mechanism from charge transfer to mass transfer, instead metal deposition behavior. Generally incorporation was maximum at the current density of 500 A/m^2 and was decreasing at higher current densities even though these values are much smaller than limiting current densities of metal [47]. By Fransaer et al. the codeposition of non-Brownian particles is described in two steps. Metal ion reduction as described by Buttler-Volmer expression and particle co-deposition. An improvement to Guglielmi’s model is brought out by Hwang & Hwang in 1993 in order to discern reduction of ions on particles. Only protons are reduced at low current densities. At medium current densities proton reduction reaches limit value and metal ions are reduced. At high current densities reduction of both protons and metal ions comes to a limit. However this model was not experimentally proven. Also they stated that three steps were included for particle incorporation. Firstly particles are being forced through cathode surface convectively, then become loosely adsorbed to surface and finally incorporation occurs by reduction of adsorbed ions [44]. Vereecken et al. stated that particle transportation through the negative electrode surface is convective diffusion controlled. However this is only valid for particles with a size smaller than diffusion layer thickness. Among all models that are above mentioned, Guglielmi’s five step model is most adoptable and it is examined on various systems [48,49].

2.3.6 Sediment codeposition

Properties of composite material are specified by volume fraction of its phases. Thermal conductivity of copper diamond composite material increases with increasing volume fraction of incorporated diamond particles [50].

In traditional composite coating techniques, concentration of reinforcement phase is not satisfying. In order to increase particle concentration in composite, sediment codeposition (SCD) method is used [51]. In this codeposition technique electrode design differs. In 1972 Viswanathan and Doss gave a new impulse to electrolytic composite production by producing metal matrix composite coatings by SCD. SCD includes a horizontally placed cathode. Insoluble particles of reinforcing phase are kept suspended in electrolyte by agitation. Agitation is recessed periodically for settlement of particles on cathode surface. By force of gravity incorporation of particles in the deposit is enabled [52].

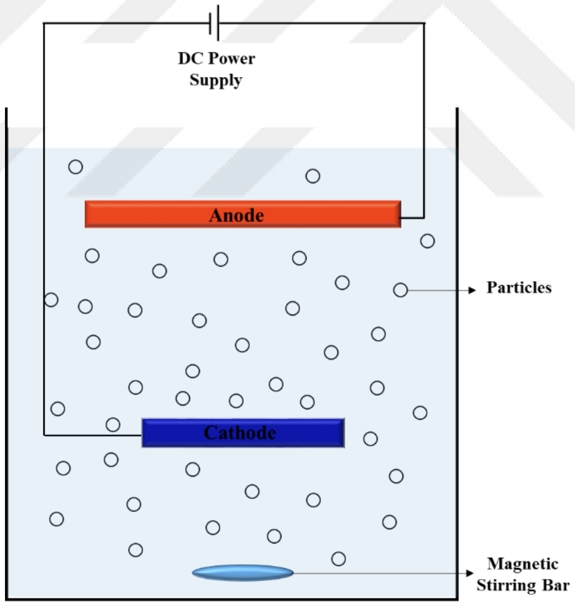

Figure 2.14 : Sediment codeposition setup illustration [53].

2.3.7 Previous studies on SCD

Jeyaraj at al. codeposited micron sized Al_2O_3 particles in nickel deposit for improvement of micro hardness by conventional deposition and sediment codeposition techniques. In their study samples then characterized by SEM, XRD and EDS for investigation of deposit. They also practiced analytical studies in order to determine the important parameters on properties of deposit. It was concluded that in CED current density and temperature; in SCD technique particle concentration of electrolyte and temperature were the parameters with greatest importance. Volume fractions of reinforcement phase are maximum 40.49% in CED method and 53.16% in SCD method. It is stated that by SCD technique microhardness value is further increased with a value of 2541 HV when it is compared to CED samples that have a maximum hardness of 1248 HV [54].

Pushpavanam et al. produced Ni-Co-Diamond composites by SCD for enhancement of tribological properties. Despite the studies in which organic additives are used to improve interface [47,55], cobalt is used as an inorganic additive to avoid detrimental properties which are resulted from organic surfactants that are used for surface modification of reinforcing particles [51]. 6-12μm sized natural diamond particles are codeposited in Ni-Co matrix. Cobalt ions are added to the bath as sulfate. The Co concentration in the alloy has a final value of 10%, the percentages are evaluated by XRF. The composite electroplating parameters which are pH, current density and diamond particle concentration of the bath are found to be effective properties on the diamond percentage in the composite deposit. Maximum hardness value of 700HV is obtained by presence of Co while Ni-Diamond composite has a microhardness value of 460HV. The improved microhardness emerges from the increment of particle fraction in deposit and decrement of agglomeration. Wear rate is found to be shrunk three times. Up to 5 g/l diamond concentration in electrolyte wear performance is enhanced however for further values a remarkable change is not observed.

Hard Ni-W-Diamond coatings by SCD technique is produced by Zhang et al. While hardness of electrodeposited Ni-W coating is also produced for comparison. It is reported that when hardness of Ni-W coating and Ni-W-diamond coating is compared, the hardness of SCD coating is higher than Ni-W coating. It is also stated that the tendency of particles to codeposit increases with increasing diamond content in the electrolyte and with increasing diamond particle size. Bath with diamond concentration of 1 g/l exhibits 960 HV while at 20 g/l 2249 HV is measured. At the highest hardness level diamond content in the deposit is 64 wt.% While the hardness shows very large increment by increasing diamond content in the electrolyte up to 5 g/l, despite increment is observed at higher reinforcement concentrations in bath, the change is not much as it might evaluated as significant [56].

According to Quin et al. composite coating for wear applications that is produced via codeposition well distributed diamond particles in Ni matrix by SCD method without any additives, has superior properties compared to one that is produced by CED. As well as reinforcement content in the composite material, distribution of the reinforcement particles is crucial for overall properties of composite. In their study Ni-diamond monolayer composite coating with diamond content of up to 72% is produced. Above this value mechanical properties are found to be worsened. The reason for worsening is linked to the agglomeration of diamond particles when diamond content in the deposit is increased. Also they observed that fully embedment of some of the diamond particles cannot be achieved. Conventional Watts bath is chosen to be electrolyte. Effect of various parameters which are diamond content in the electrolyte, current density and temperature is observed. With increasing diamond content in bath, diamond content in the deposit is increased [57].

3. EXPERIMENTAL STUDIES

The initial aim for producing enhanced copper-diamond composites is to design an electroforming system by which samples can be fabricated with the desired geometry and dimensions. Experimental studies section begins with the projection of the electroforming system design. In the following subsections, experimental procedure; including optimization period of the electrolyte constituents and operation parameters is presented. Details of applied post treatments are indicated. Structural and mechanical characterization results of as deposited and post treated samples along with the encountered problems throughout experimental studies and their solutions are also revealed in this chapter, under results and discussion section.

3.1 Electroforming System Design

In SCD technique a regular composite material is obtained through the steps of bending a conductive metal in L shape, addition of reinforcement particles to the electrolyte, agitation of particles through stirring, settlement of the particles on horizontal site of the bent metal and initiating electrodeposition. However, such a simple system is unacceptable as a reliable manufacturing technique. The main reason is the lack of precision. One of the other reasons is that the material loss would be dramatic. Not only the anode metal will be unnecessarily deposited on irrelevant sites but most of the cathodic area will be scrap since composite is only obtained from the areas where particles are settled. In previous studies, cathode surfaces have been isolated by painting or polymer coating and then the plated area is sectioned from the cathode surface. The left over painted cathode requires a mechanical work for being re-used, or another cathode is used again by making it partially nonconductive. In order to avoid waste of resources and vain effort, a practical system is required for the use in electroforming. The most important part of an electroforming system that needs to be well modified is the cathode. Designing a cathode system minimizes the preliminary efforts, waste of material and it is also enables the achievement of near net shape composites with desired thickness. First aspect of such design is making it impermeable to the electrolyte. The only electrically conductive area in contact with the electrolyte must be the substrate surface. If any other sites of the system is conductive, it will be copper coated. In that case, the current density, which is a critical parameter for electroforming, will change and sample morphologies will be unintentionally affected. In composite electroforming setups, another prerequisite is that reinforcing particles must settle on the substrate surface prior to polarization. The settled particles must cover the substrate surface with a homogeneous distribution. Considering these factors a suitable and practical system is designed. In the designed electroforming system, a lid with a hole in the center is used to gather the reinforcing particles together in a circular form. The idea behind this action was to put the substrate underneath the lid and to initiate electroforming process on the substrate. As electrodeposition continues, reduced copper ions fill the gaps between the diamond particles and form the copper-diamond composite. With designed setup, unlike previous studies, a practical method is established and same system can be re-used each time. Moreover, fabricated composite can have the desired near net shape with the lid system. Elements that constitute the cathode system are designated in Figure 3.1.

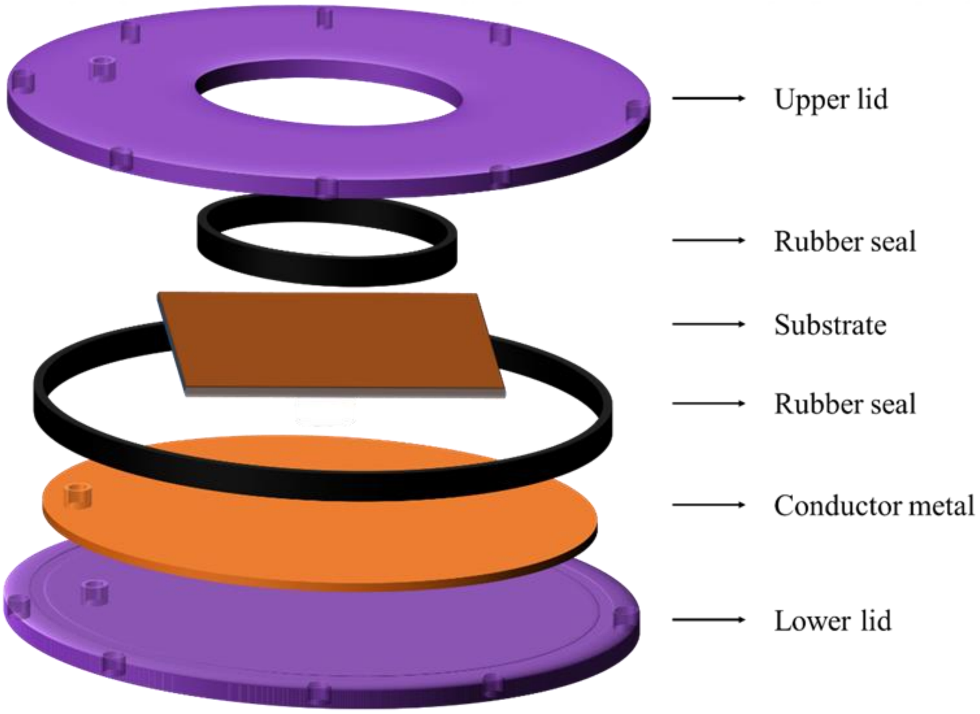

Figure 3.1 : Compartments of the cathode system.

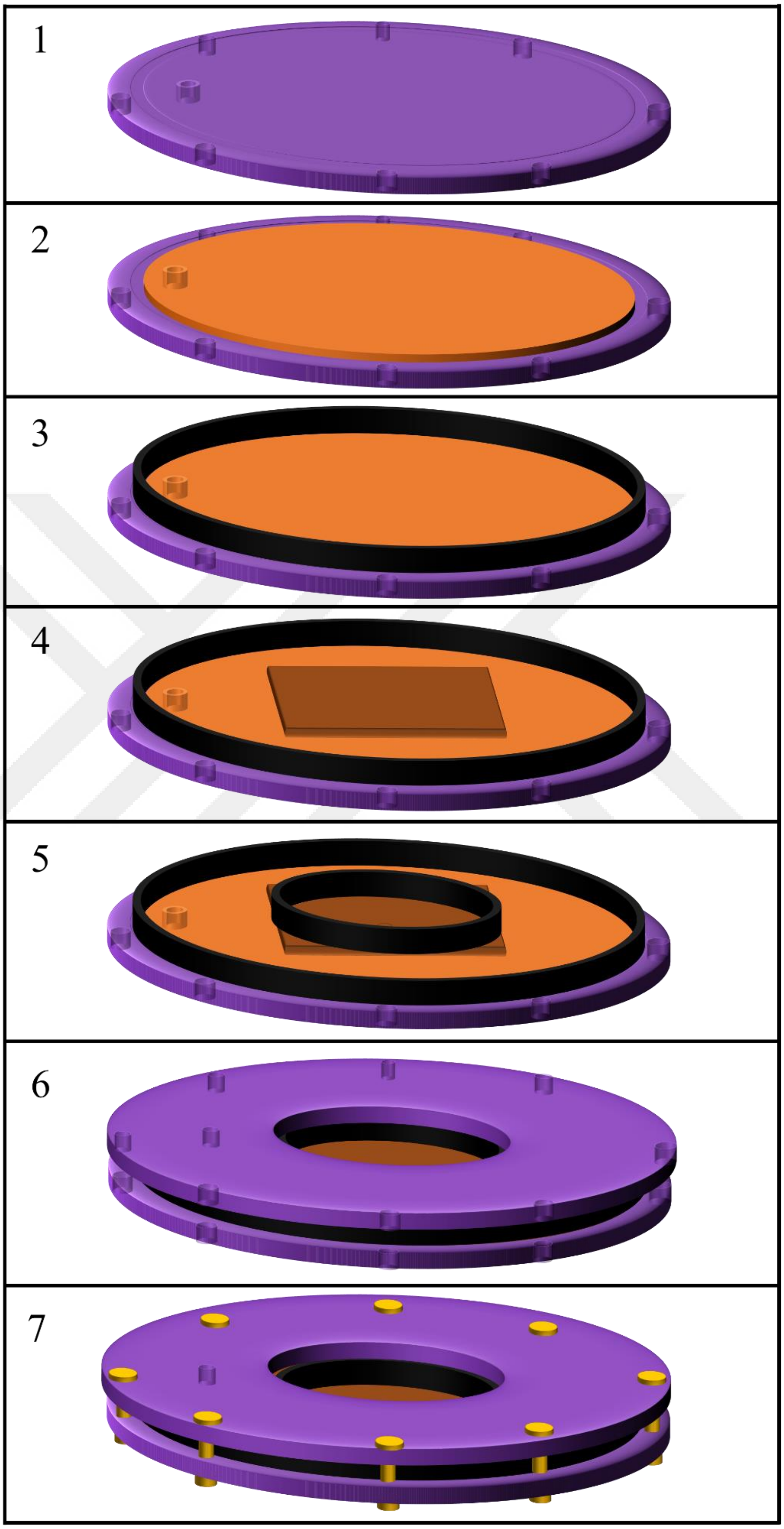

Figure 3.2 : Sequence of assembly for the cathode system.

The upper and lower lids are made of Plexiglas, which is a polymeric material. The reason of selecting Plexiglas is that it does not react with the electrolyte and it is nonconductive. Plexiglas also has the strength to withstand stress from compression without fracturing and maintaining its rigidity. Identical holes present at the edges of both lids are for inserting screws and bolts for compression. The hole in left hand side of the center in both lids are for the entrance of the threaded rod. Lower lid has a channel carved on the surface to fit the rubber seal. Circular metal plate is made of copper and used for conducting the current to the substrate, which is the square shaped copper plate. There is also another rubber seal used for compressing the substrate. The larger hole in the upper lid is for settling the diamond particles on the substrate surface. That part is filled with the electrolyte afterwards. The fabricated composite will grow in that prepared hole while taking the identical shape of it.

Sequence of assembly for the compartments are shared in Figure 3.2. First, the lower lid is taken. Conductor copper plate is put above it. Then, larger rubber seal is fixed on the carved part in lower lid. Afterwards, copper substrate is placed at the center on conductor metal. The other rubber seal is fixed right above the substrate. Finally, the upper lid is put above the parts and system is compressed by using plastic screws and bolts.

As it is shown in Figure 3.3, the experimental setup fundamentally consists of a cathode and an anode, which are connected to the negative and positive ends of a power supply respectively, imbedded in the electrolyte. Current is conducted to both electrodes by a steel threaded rods isolated with heat shrink tubes.

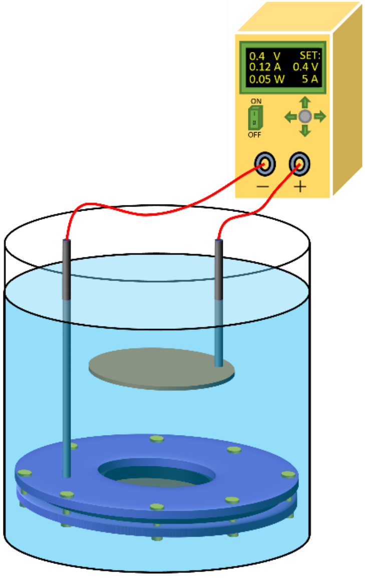

Figure 3.3 : Illustration of the experimental setup.

3.2 Experimental Procedure

In order to achieve the strongest possible matrix-reinforcement interface, SCD technique is selected and modified to electroforming. As the initial step, a traditional acid copper sulfate plating bath is prepared with brightener addition. Electrolyte composition is given in Table 3.1.

Table 3.1 : Copper-diamond composite electroforming bath.

Bath ingredient	Conc. (g/L)
Copper sulfate	180
Sulfuric acid	30
Hydrochloric acid	0.1
Thiourea	0.05

Diamond particles with particles sizes 75 and 250 μm are used in different baths. The presented electroforming system is used throughout the electroforming experiments.

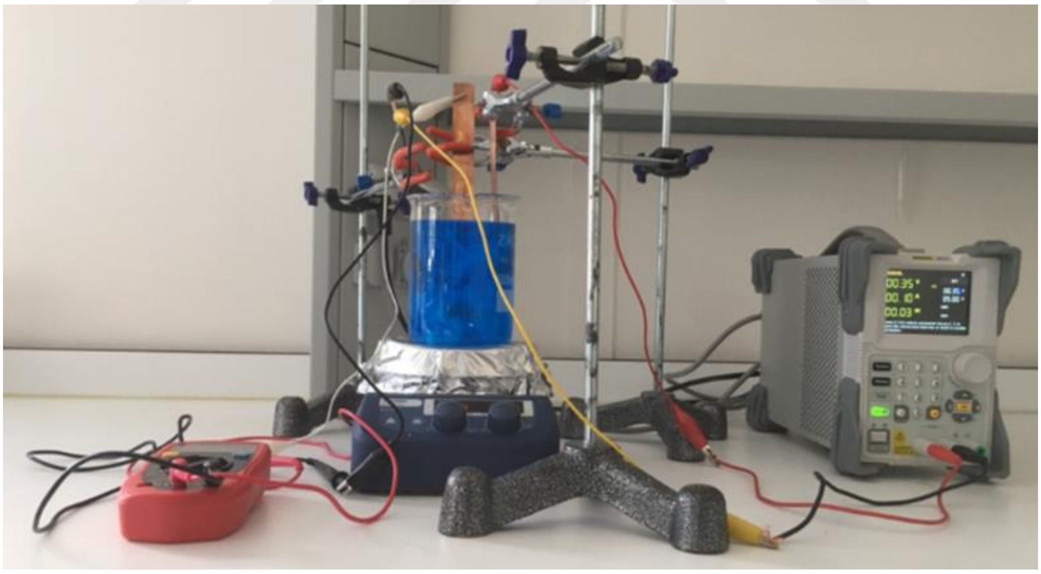

Figure 3.4 : Copper-diamond electroforming setup.

Before mounting the substrate on the cathode system, each sample was grinded with sand papers, pickled with %15 sulfuric acid, rinsed with acetone to remove the grease and oxide layers and obtaining a smooth surface. During the experiments, a voltmeter continuously measured the potential difference between the working electrode and the reference electrode. Optimized operation parameters are given in Table 4.2. In order to optimize the electroforming parameters, polarization curve of the electrolyte was drawn by a potentiostat and different trials were conducted under various current densities.

Table 3.2 : Optimized operation parameters of copper-diamond electroforming.

Operating conditions	Value
pH	0.5
Temperature	40 °C
Current type	DC
Applied voltage	300 mV
V (WE vs. RE)	160 mV
Current density	1 A/dm^2
Agitation	Magnetic stirring
Particle size	75 - 250 µm

With the optimized parameters, different composite samples were fabricated with particle size 75 and 250 µm. For trapping diamond particles inside the composite structure, in other words, for copper ions to travel through the diamond particles by the electrolyte, different particle settlement methods were tried. First experiments were done by pouring 0.5 g dry diamond particles inside the hole of the upper lid. Following experiments were conducted by initially soaking the diamond particles in a solution containing the same composition with the forming electrolyte till they are completely wet, then filling the hole with the wet diamond particles.

Optimization procedure was done by fixing one layer of 250 µm diamond particles on the substrate surface by plating at various current densities in durations ranging between 2-4 hours. In these trials, the duration is kept deliberately short so that the surface of the reinforcing particles would not be coated with copper and the distribution of diamond particles could be analyzed. After the operating conditions are optimized, as the next step, electroforming duration is extended to 30 hours to initiate the surface covering of diamond particles with pure copper.

After composite electroforming became a reproducible method where diamond particles were homogeneously incorporated inside the copper matrix and the surface was coated with pure copper, in order to enhance the interface between copper matrix and incorporated diamond particles, a group of samples were annealed, a group of samples were cold isostatic pressed and a group of samples were both annealed and cold isostatic pressed. Annealing was conducted at 650 °C for 2 hours while cold isostatic pressing was done under 1.5 x 10^6 N pressure.

Scanning electron microscopy imaging were performed on as deposited and as treated samples for investigated the matrix-reinforcement interface, to analyze the smoothness of deposited copper and to detect the volume fraction of incorporated diamond particles.

X-Ray diffraction patterns of each sample were plotted to investigate the structural properties of as deposited sample and to investigate the changes induced by annealing and cold isostatic pressing on the matrix-reinforcement interfaces.

Finally, for being able to comment on the formability of fabricated composites, three point flexural tests were conducted for as deposited and as annealed samples.

3.3 Results & Discussion

Results and discussion chapter begins with description of encountered problems during initial electroforming attempts. The way how each problem was solved is detailly explained. After eliminating the troubling aspects of electrodeposition, composites with desired properties were fabricated. Visual, structural and mechanical characterizations of samples are given in the following subchapters.

3.3.1 Process optimization

After the experimental setup was established and the electrolyte was prepared, the first electroforming trial was conducted by pouring 250 μm diamond particles into the hole on the substrate as seen in Fig. 3.5. Regardless of the operating parameters, the results for the first attempt were a failure. The reason behind this was thought to be the inability of electrolyte to infiltrate through the diamond particles and contact the substrate surface. This situation was caused by the unwetted diamond particles. After pouring dry diamond particles into the hole and embedding it into the electrolyte, only the particles at the top surface were wetted and electrolyte could not leak the particles at the bottom site. Diamond particles floating on the electrolyte surface also verified

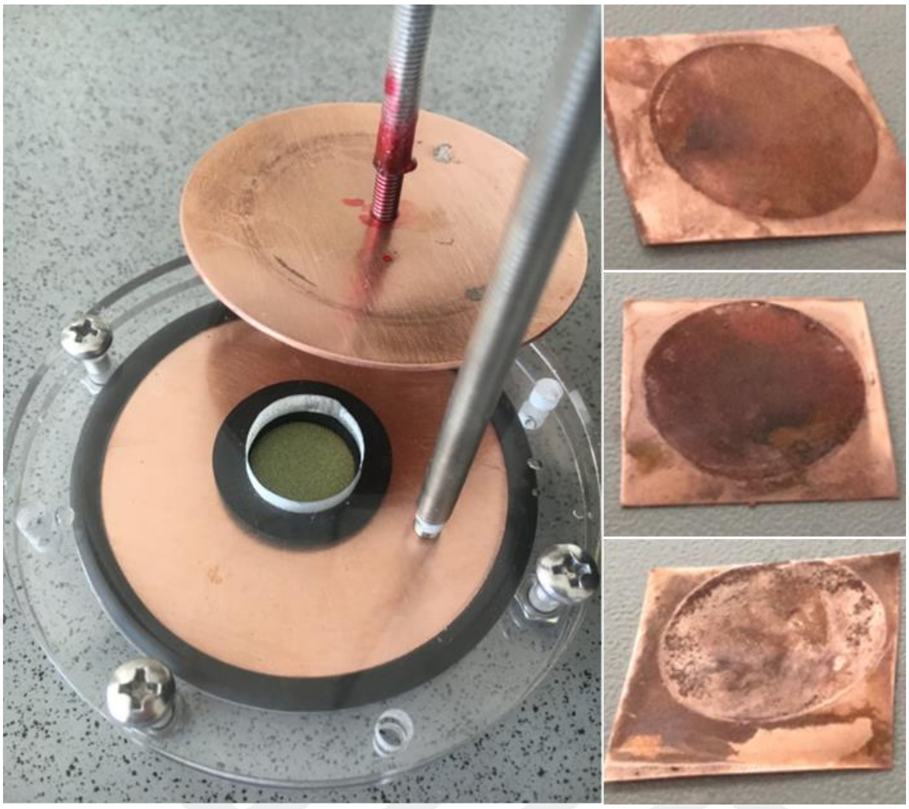

Figure 3.5 : Settled diamond particles inside the hole on the designed cathode system (left), samples from the first electroforming attempt (right).

this idea. After particles were dipped into the electrolyte, some dry diamond particles formed clusters and elevated to the solution surface. Clusters of unwetted diamond particles are shown in Fig. 3.6.

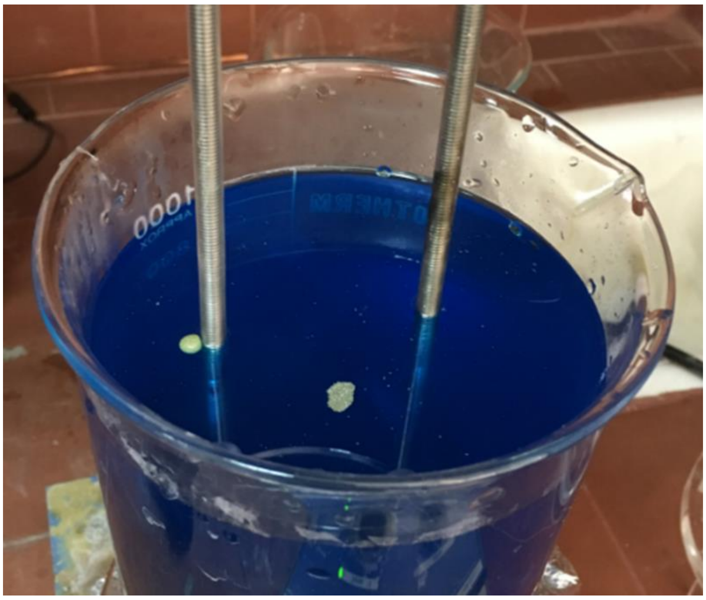

Figure 3.6 : Diamond particle clusters floating on the electrolyte surface.

Although this problem completely prevents reinforcing incorporation, a simple solution was implemented. In order to enforce the electrolyte to infiltrate through the particles, diamond particles were initially wet in a solution identical to the forming electrolyte. The wetting procedure continued till there were no clusters floating on the electrolyte surface. Mixing was started first mechanically by magnetic stirrer and afterwards continued in ultrasonic bath. Afterwards, wet diamond particles were taken from the solution and poured on the substrate.

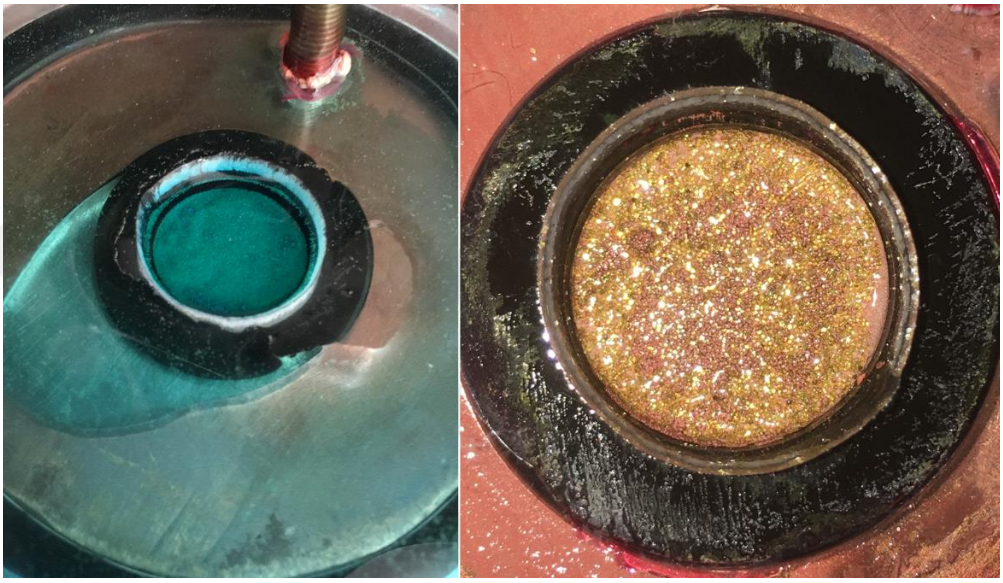

Figure 3.7 : Usage of pre-wet diamond particles.

By using wet diamond particles, electrolyte was able to be infiltrate through particles and reach substrate surface. Several samples were fabricated by traditional operating conditions for pure copper electroforming procedure, the only different parameter from table 4.2 being the adjustment of current density. The current density was calculated by estimating the conductive cathodic area and current was supplied accordingly to fix the current density at 1 A/dm^2. At that point, diamond particles were able to be trapped by deposited copper, however the next challenge was encountered.

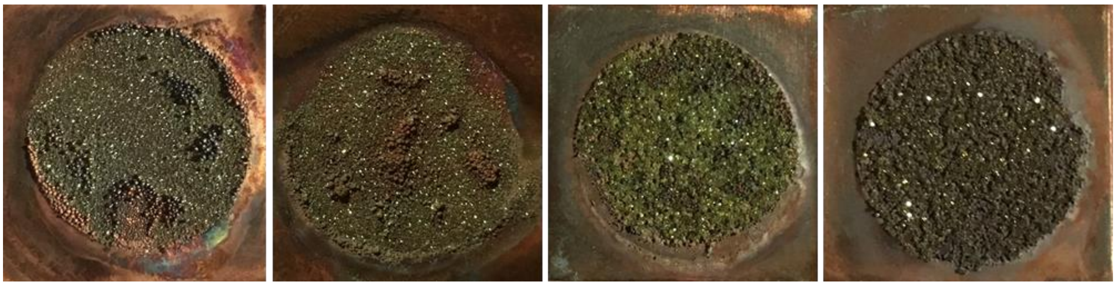

Figure 3.8 : First set of samples formed by using wet diamond particles.

The new challenge was that; in the following experiments, fabricated composites were not bright and they had dendrites growing around some nucleation sites. Smooth copper deposition was not obtained. Due to the dendritic growing, diamond particles at these sites were not incorporated in copper matrix, instead they were thrust by dendrites sideways. The hypothesis regarding dendrites thrust diamond particle instead of growing while surrounding them smoothly is proven by scanning electron microscopy imaging.

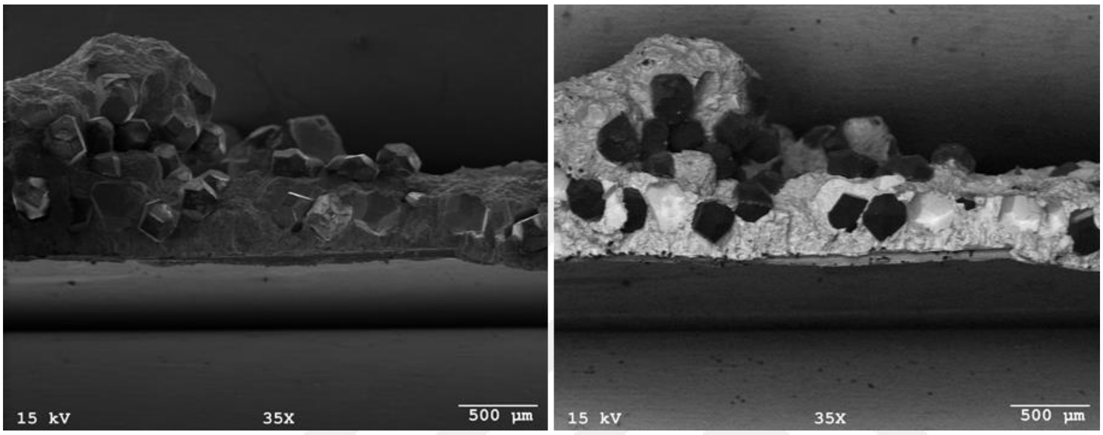

Figure 3.9 : SEM images of copper-diamond composite cross-section at 35X mag. with secondary electrons (left) and back-scattered electrons (right).

From scanning electron microscopy images of composite in Fig. 3.9, the mound on the left hand site can be analyzed. At the mound it is seen that the level of diamond particles are elevated. As copper was deposited it did not wrap the diamond particle but instead lifted them while pushing them. Right after copper deposition starts, the diamond particles were levelled. But at the end of electroforming, diamond particles came together at the edge of the mound and were lifted. This is not tolerable. The primary aim for having a functional composite is to obtain a morphology, in which deposited copper only should fill the gaps between diamond particles. Although particles will under any circumstance slightly dislocate due to the stresses induced by deposition, it should in all cases wrap particles thoroughly down to the last detail and dendritic growth is not acceptable.

From literature overview, it is well known that the most critical parameters affecting deposit morphology in electroforming are electrolyte and its additives, temperature and current density. With current electrolyte and operating conditions, without adding reinforcing particles bright and smooth copper plating was achieved. The only variable among critical parameters when adding diamond particles to the equation is the current density. As shown in Fig 3.5, when diamond particles contact with substrate, they isolate that area. Therefore, the substrate surfaces in touch with diamond particles are not conductive anymore. Moreover, as copper deposits, new conductive and nonconductive areas emerge. As a result, when steady current is applied to the system from power source, current density changes instantaneously through the process due to the change in the conductive area. For a proper process, current density must be fixed. As a solution, instead of applying steady current, it is decided to switch to potential controlled setup. If fixed potential difference is applied, then the current changes according to the surface area. Assuming that the initial conductive area covers a quarter of the entire area when diamond particles are settled on substrate surface, if steady potential is applied, both the conductive area and passing current will be low, but as copper covers the entire substrate surface, the passing current and the conductive area will increase. Since current density equals current passing through unit area, current density will remain steady during the process.

Although switching to potential controlled system can fix the current density, it is still a challenge to calculate the actual current density by measuring the cathodic area due to isolated sites by settled particles. Here, in order to solve this polarization curve of the electroforming bath is plotted.

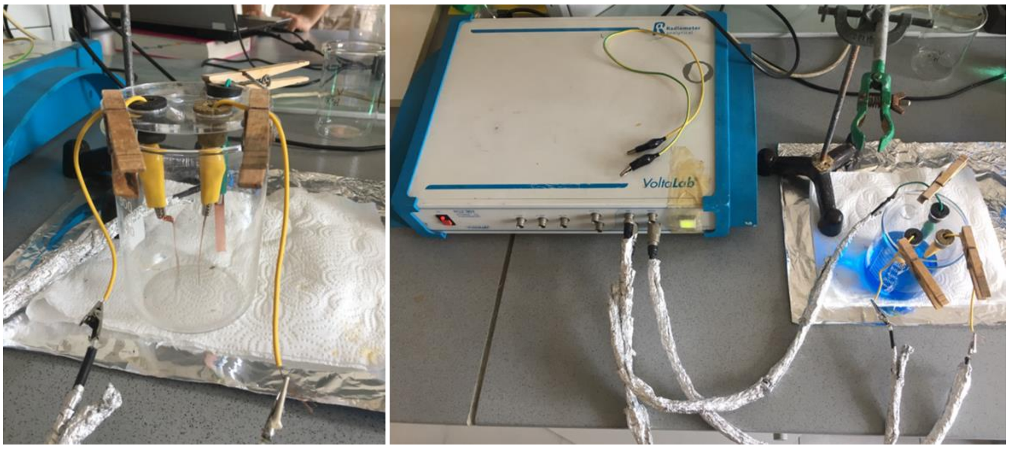

Figure 3.10 : Three electrode cell (left) filled with electroforming bath to plot the polarization curve with potentiostat (right).

The three electrode cell for polarization curve consists of three copper strips which are cut from the same plate used during experiments. Since the anode and the cathode are both copper and the bath is acidic copper sulfate bath, using copper as reference electrode provides stability and it does not generate potential in the cell. Therefore copper is selected as reference electrode.

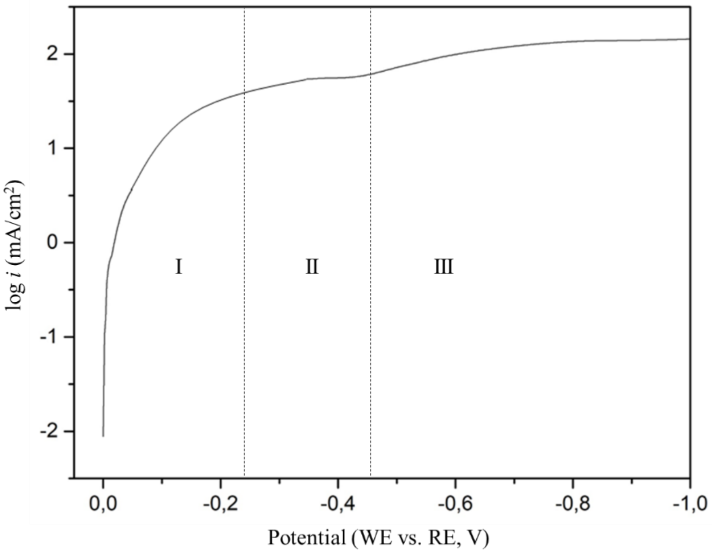

Figure 3.11 : Polarization curve plotted in process bath indicating regions where I: Activation controlled, II: Mixed controlled, III: Diffusion controlled.

Polarization curves are usually plotted to calculate the threshold for transition to diffusion controlled mechanism from activation controlled which are shown as regions I and III in Fig. 3.11. From literature it is already known that current density interval of 1-2 A/dm^2 fulfills bright metal deposition, enables the wrapping of diamond particles till their last detail. The main reason for plotting polarization curve is detecting which potential difference corresponds to a current density of 1 A/dm^2. From polarization curve data it is found that 160 mV potential difference between the cathode and the copper reference electrode corresponds to a current density of 1 A/dm^2. After that point, during electroforming procedure, a voltmeter was used. The clips of voltmeter were attached to the cathode and the copper reference electrode.

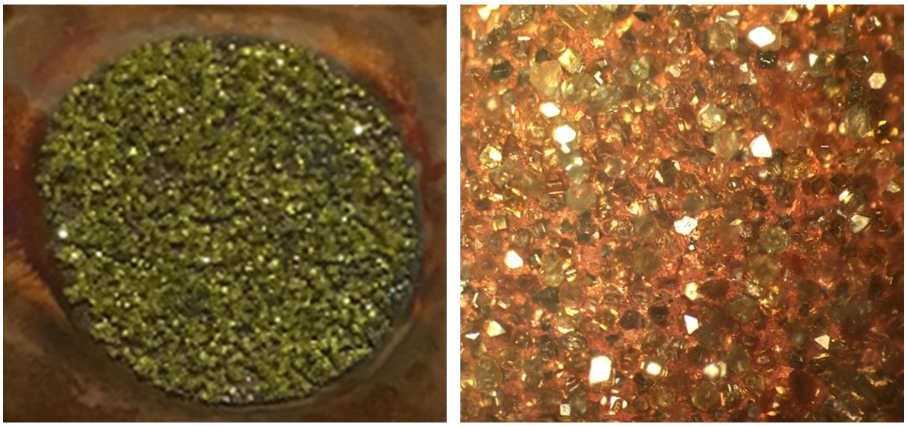

Figure 3.12 : Macroscopic and optical microscope image of sample fabricated with potential controlled system

When applying potential difference to the cathode and the anode, the potential difference between cathode and the reference electrode was measured. Potential from the power supply is adjusted to 300 mV since at that voltage the voltmeter measured 160 mV potential difference between cathode and the reference electrode. By switching to potential controlled system and adjusting the mentioned potential difference, another composite is fabricated. The composite formed by potential controlled system exhibited a levelled surface, although elapsed time for plating was 2 hours, deposited copper was enough to wrap the diamond particles strong enough that they remain attached to the substrate. The sample was then sectioned for its surface and cross-section to be imaged by SEM and EDS analysis was also conducted to see if there were any impurities.

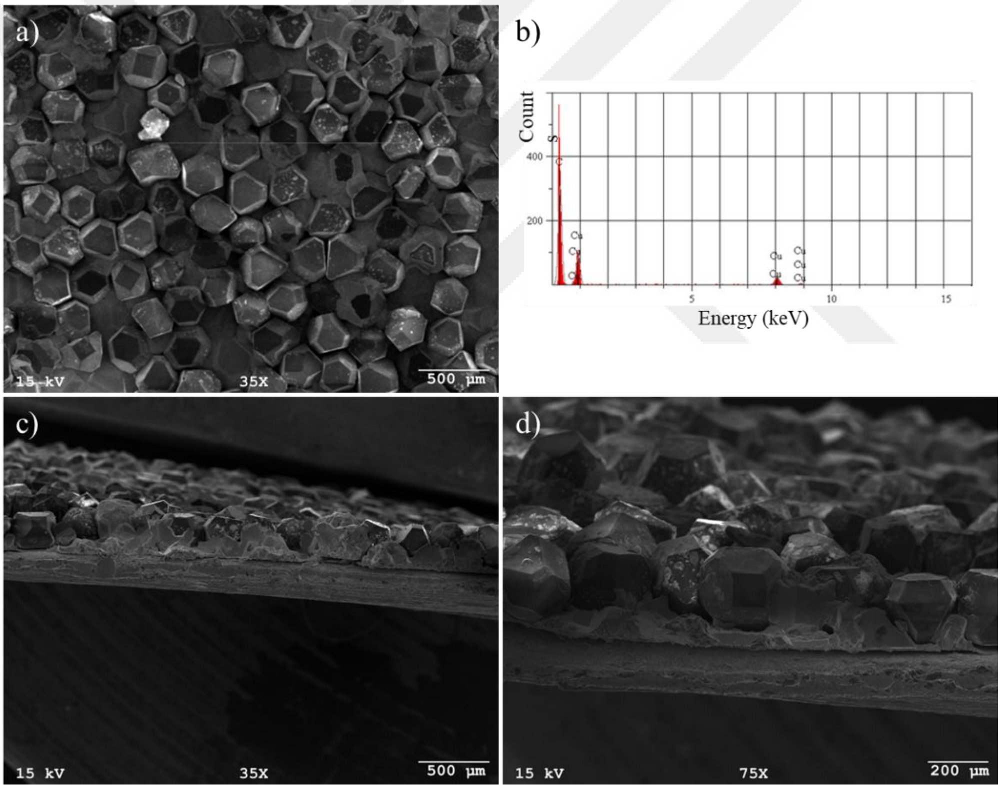

Figure 3.13 : Characterization of the first sample fabricated by potential controlled system; a) SEM image of surface with SE at 35X mag. (b) EDS analysis, (c,d) SEM images of cross-section with SE at 35X, 75X mag.

SEM images of the sample verified that unlike previous attempts, after switching to potential controlled system the copper deposition was smoother and no mounts were present. Deposited copper filled the gaps between reinforcing diamond particles and wrapped them as it can be seen from images of the cross-section. In the next part, the electroforming duration is extended to 30h for completely covering the surface by copper and incorporating every settled particle inside the structure.

First 30h ongoing electroforming was conducted by 75 µm diamond particles. At the end of 30 hours, copper-diamond composite with a surface entirely copper coated was retrieved from the cathode system. Surprisingly, by applying delicate pressure by hand to the edges of substrate, the pure electrolytic composite was completely separated from it.

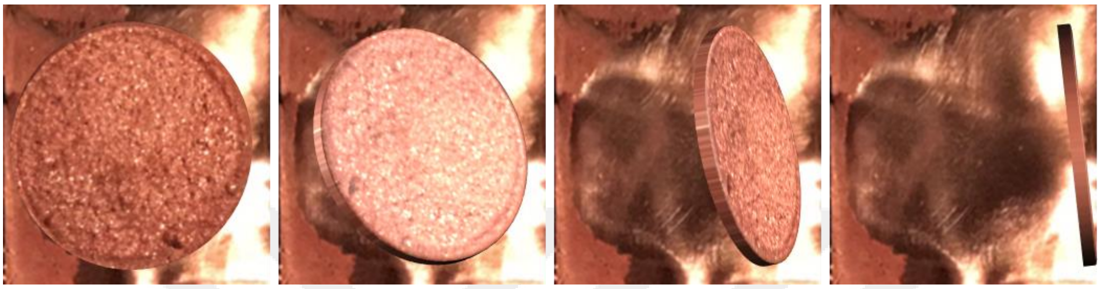

Figure 3.14 : Lifting the composite from substrate.

This non-destructive separation possibility is discovered in this study. In literature, researchers either mechanically strip the electroformed material from the substrate or they chemically dissolve the substrate. While eliminating material loss, this brings the process practicality. Most important of all, the bottom surface of the composite is observed to be the negative identical shape of the substrate. By this means, when a polished substrate is used, the bottom surface of the composite will also be polished.

Afterwards, another composite with a diamond particle size of 250 µm was fabricated with same operating conditions. This composite was also easily detached from the substrate. At this moment the electroforming operation parameters are optimized to set the goal of fabricating a copper-diamond composite.

3.3.2 Surface imaging of as deposited samples

Surfaces and cross-sections of both samples were characterized with scanning electron microscopy. The first point to analyze is the interface between copper matrix and diamond particles. The dispersion homogeneity of diamond particles and deposited copper morphology must also be investigated. Moreover, from SEM imaging, composite thickness and volume of incorporated diamond particles will be calculated. For as deposited samples, the bottom surface of composites which used to look at the substrate are also investigated.

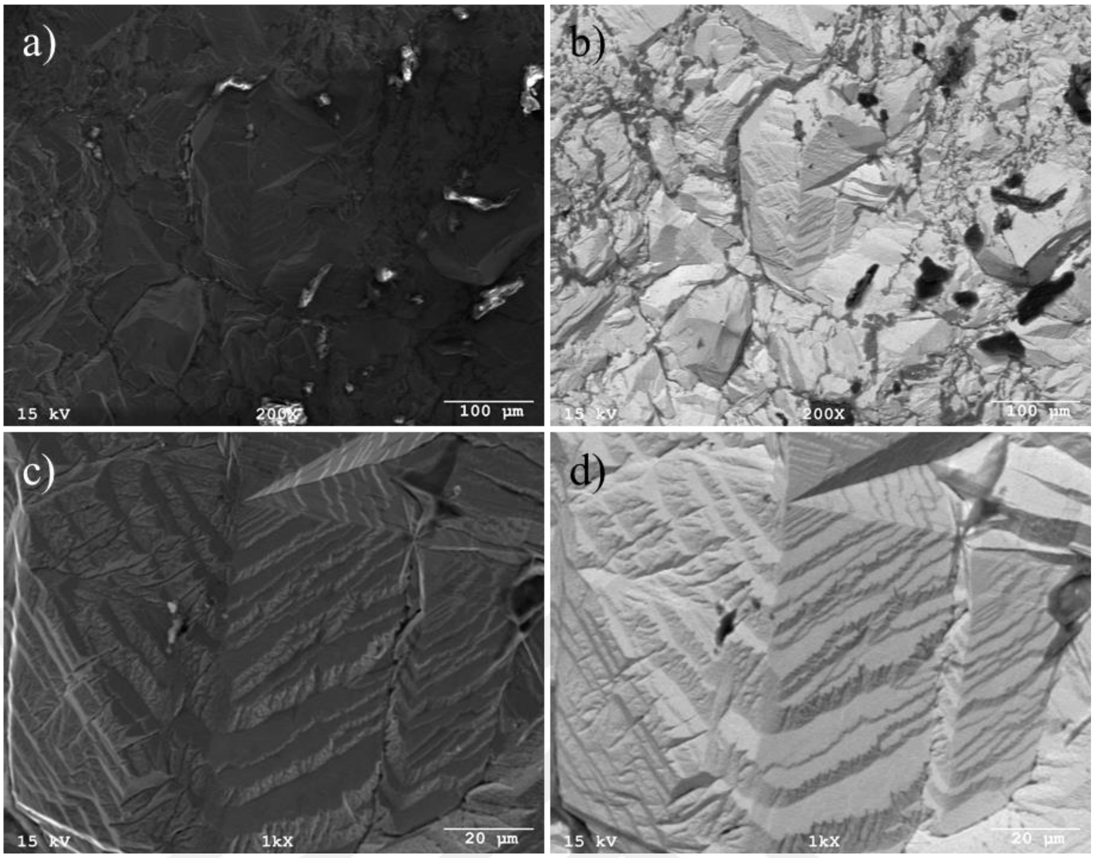

Figure 3.15 : SEM images of sample surface with 250 μm diamond particles; (a,b) at 200X with SE, BSE respectively, (c,d) at 1kX with SE, BSE respectively.

Marvelously, SEM images shared in Fig. 3.15 reveal that copper was deposited on diamond particles so smoothly, it took the identical shape of it. The deposited copper has diamond facets. In other words, copper atoms precisely wrapped the reinforcing particles.

In Fig. 3.16, the sample was mechanically cut into two sections from half in order to analyze its cross-section. During sectioning, some particles naturally were detached from the structure. When looking at cross-sections, it is very easy to detect the holes left behind by diamond particles. This occurrence validates the previous theory regarding copper precisely covering the diamond particles. Since copper smoothly coats the reinforcing particles and traps them, once a particle is lifted, the shape it leaves behind is its original structure. Hence, copper was even able to retrieve the shape of diamond facets. The undesired occurrence seen from the cross-sections in Fig. 3.16 with 250 μm particles is that particles are in contact through a layer. Since they are not separated by matrix it is highly probable that there are pores between the reinforcing particles which may negatively affect the thermal conductivity.

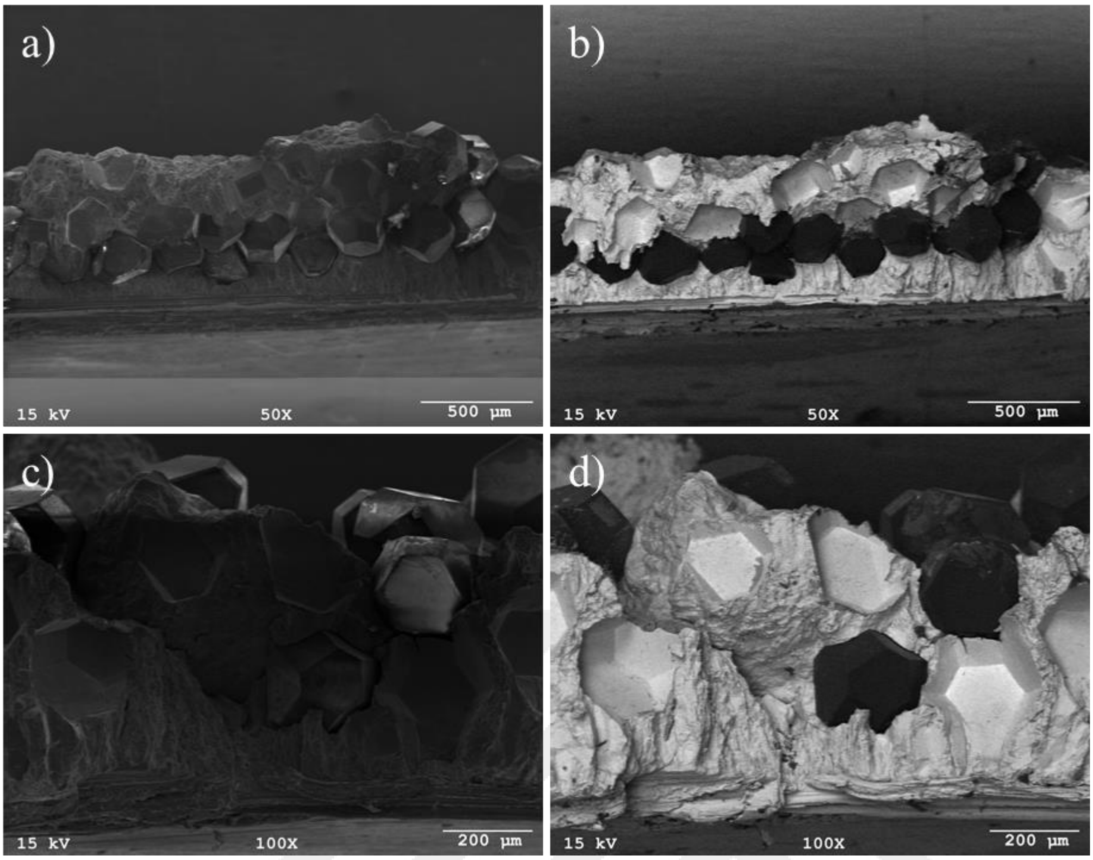

Figure 3.16 : SEM images of sample cross-sections with 250 µm diamond particles; (a,b) at 50X with SE, BSE respectively, (c,d) at 100X with SE, BSE respectively.

Cross-section imaging from Fig. 3.17 revealed that composite with 75 µm reinforcing particle size is much more demanding than the one with 250 µm. The top surface is levelled and the homogeneous and frequent distribution of diamond particles are spectacular. Considering that a respectable amount of diamond particles were detached during sectioning, even the number of remaining particles are satisfying.

Moreover, unlike the previous sample, in composite with 75 µm reinforcing particle size particles are mostly not in contact with each other. They are separated by the copper matrix. The composite thickness is measured 728.2 µm. This thickness is reached after 30 hours of electroforming, which can be considered as a disadvantage compared to other production methods. However, for a heat exchanger material, thicknesses around 1000 µm is viable. This thickness can be reached with current bath around 40 hours, but by increasing the current density and modifying additives it can be shortened. In Fig. 17 c and d, sample is tilted by 30°. By this way, the bottom surface of the composite is revealed.

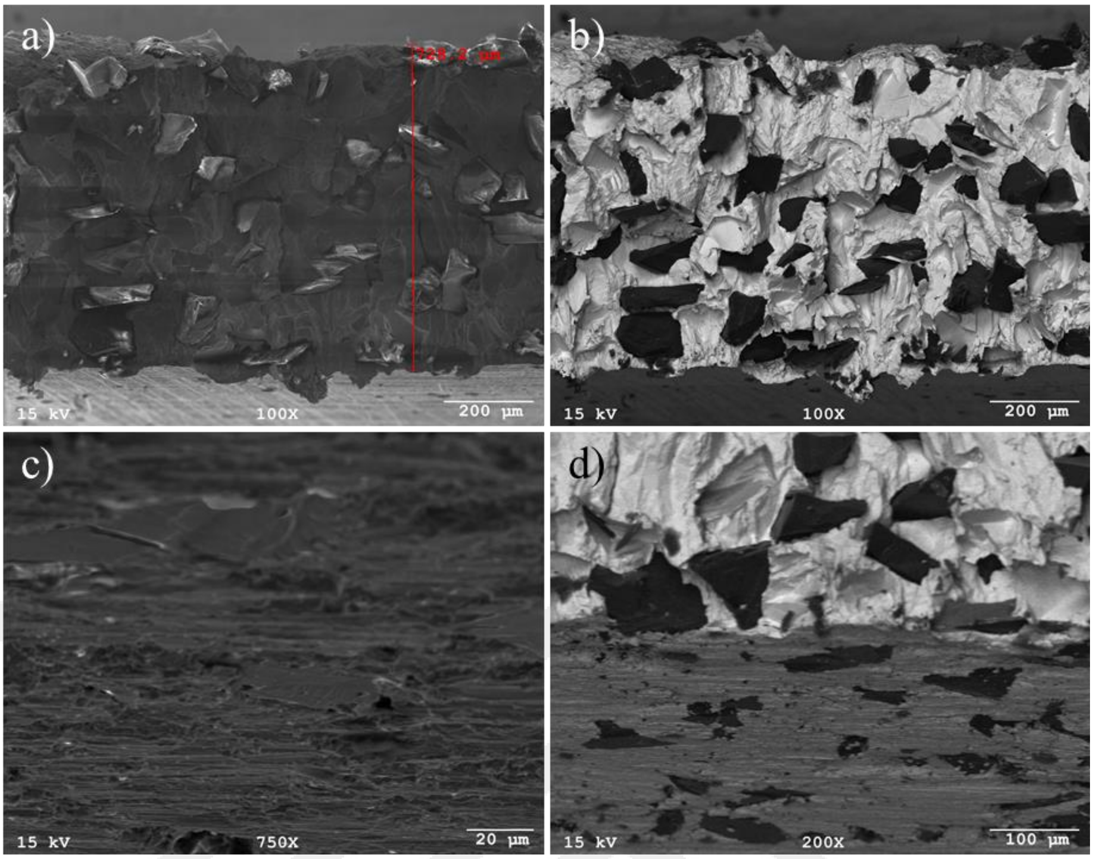

Figure 3.17 : SEM images of sample cross-sections with 75 µm diamond particles; (a,b) at 100X with SE, BSE respectively, (c,d) 30° tilted at 750X, 200X with SE, BSE respectively.

Bottom surface is the surface which was attached to the substrate during electroforming. Diamond particle tips can be seen from the bottom surface. This explains why composite was able to be easily detached from the substrate. Before electroforming begun, tips of the settled diamond particles were in contact with the substrate. During electroforming, copper filled the bottom layer but due to the diamond tips it never completely surrounded the cathode surface. Another detail about bottom surface is that grinding marks of substrate has passed to bottom surface. Copper was initially deposited by precisely coating the substrate. During this incidence, deposited atoms took the negative image of the surface underneath them. Since the substrate was pretreated by grinding, there were remaining scratches, which are seen parallel to the bulk material. The reason why the size of diamond particles vary at the bottom surface is related to their initial positions during particle settlement. Additionally, 75 µm diamond particles do not have a specific geometry or the facets present in 250 µm diamond particles. However, this may be the reason why they are distributed at a higher extent.

3.3.3 Surface imaging of post treated samples

Surfaces and cross-sections of annealed, cold isostatic pressed, both cold isostatic pressed and annealed samples are characterized by scanning electron microscopy. The main purpose of performing these post treatments is to enhance the matrix – reinforcement interface strength by eliminating the pores, which can be identified by SEM imaging.

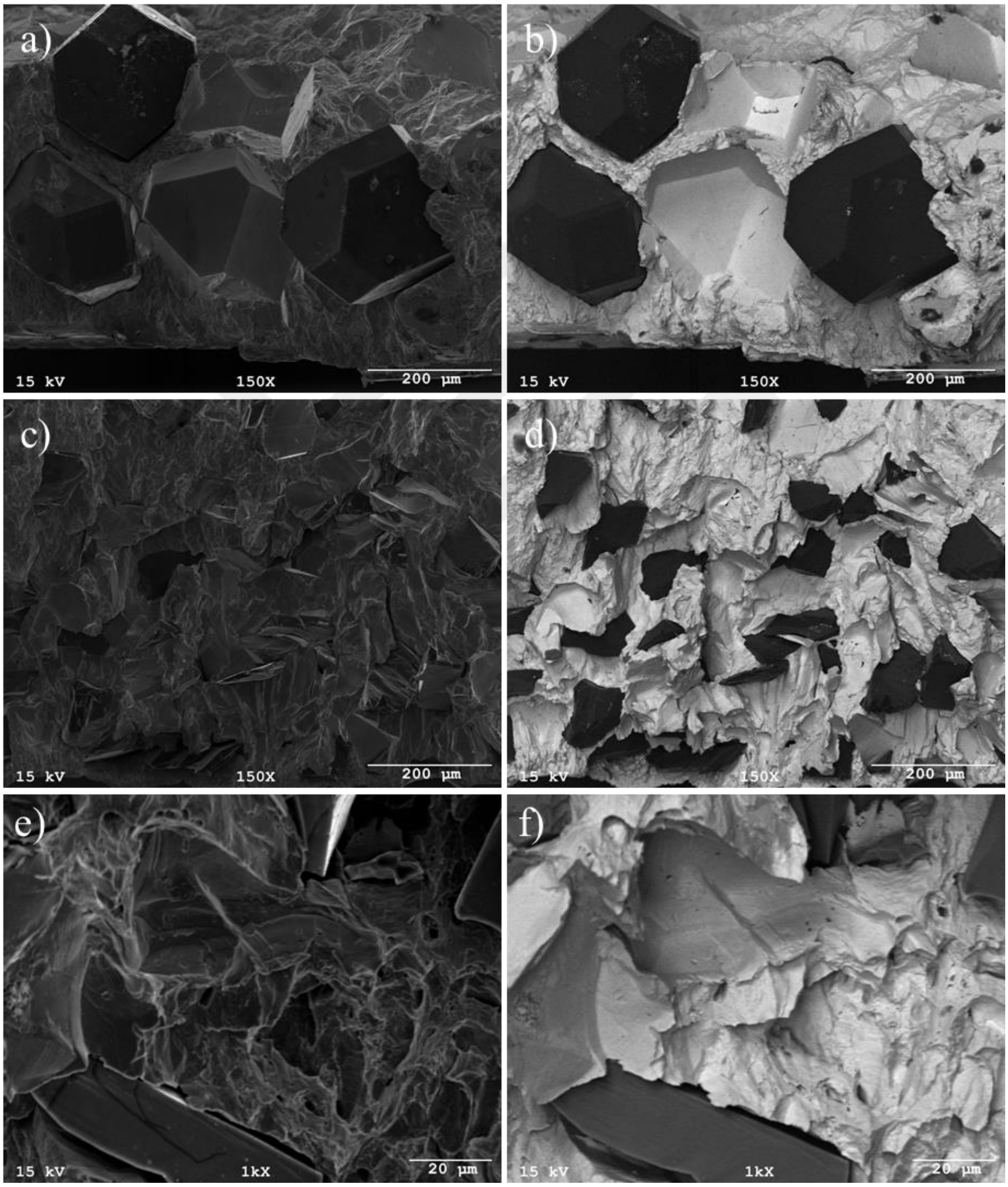
a)
15 kV
150X
200 µm
b)
15 kV
150X
200 µm
c)
15 kV
150X
200 µm
d)
15 kV
150X
200 µm
e)
15 kV
1kX
20 µm
f)
15 kV
1kX
20 µm

Figure 3.18 : SEM images of annealed samples cross-section; (a,b) 250 µm particles at 150X with SE, BSE resp. (c,d) 75 µm particles at 150X with SE, BSE resp. (e,f) 75 µm particles at 1kX with SE, BSE resp.

SEM images of annealed sample cross-sections revealed that annealing did not have a visible effect on the interfaces. The voids at the interface remains almost identical to the as deposited sample. As it can be seen from the images in Fig. 3.19 and 3.20, Cold isostatic pressing however had a distinct influence upon the structure.

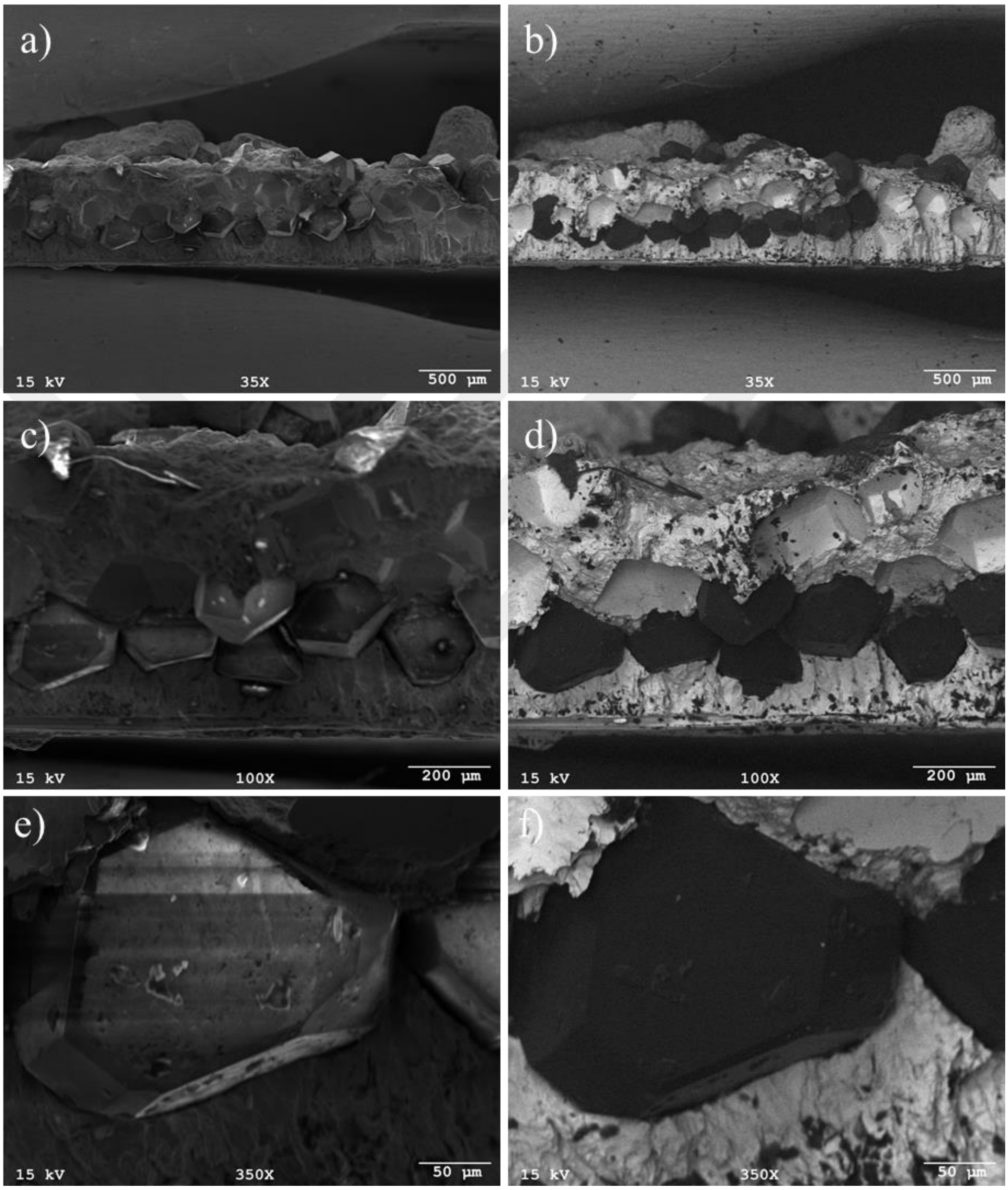
a)
15 kV
35X
500 µm
b)
15 kV
35X
500 µm
c)
15 kV
100X
200 µm
d)
15 kV
100X
200 µm
e)
15 kV
350X
50 µm
f)
15 kV
350X
50 µm

Figure 3.19 : SEM images of CIP’d samples cross-sections with 250 µm particles, (a,b) at 35X with SE, BSE resp. (c,d) at 100X with SE, BSE resp. (e,f) at 350 X with SE, BSE resp.

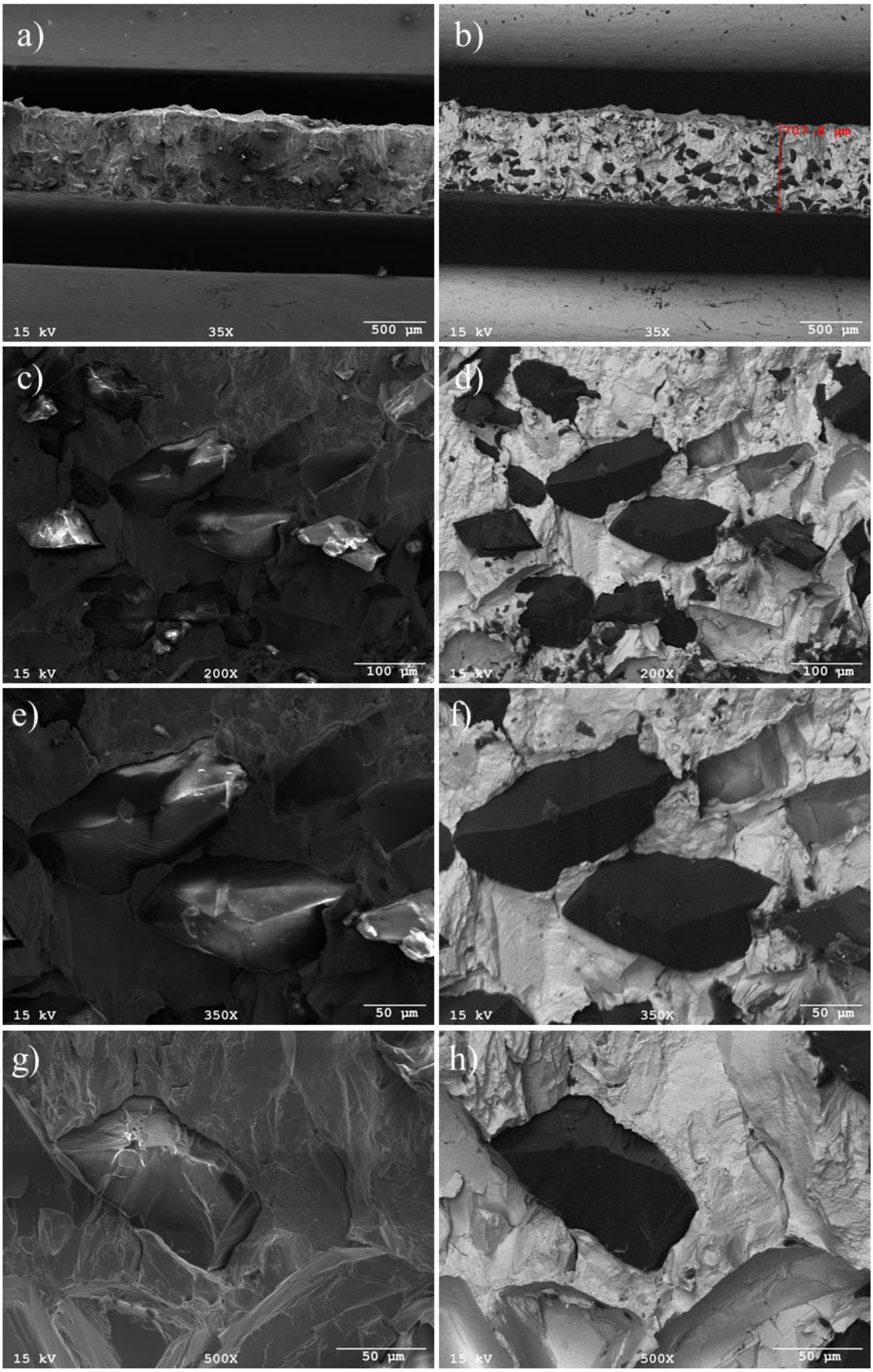
a)
15 kV 35X 500 µm
b)
707.8 µm
15 kV 35X 500 µm
c)
15 kV 200X 100 µm
d)
15 kV 200X 100 µm
e)
15 kV 350X 50 µm
f)
15 kV 350X 50 µm
g)
15 kV 500X 50 µm
h)
15 kV 500X 50 µm

Figure 3.20 : SEM images of CIP'd samples cross-sections with 75 µm particles, (a,b) at 35X with SE, BSE resp. (c,d) at 200X with SE, BSE resp. (e,f) at 350 X with SE, BSE resp. (g,h) at 500X with SE, BSE resp.

In Fig. 3.19, it is seen that after cold isostatic pressing revealed smaller diamond powders which were underneath the cross-section. In Fig 3.16, same area of the as deposited sample was investigated however these diamond particles are not present in that image. It was earlier mentioned that the diamond particles contained diamond dust and EDS analysis showed that they are not impurities. The reason why the smaller diamond particles came to the surface can be explained by the difference in hardness of matrix and composite. Diamond is known as one of the hardest materials on earth. Copper on the other side is a soft metal. During cold isostatic pressing, pressure was applied on each point of the composite. At that pressure, softer copper crept through composites center. However, hard diamond particles remained their first location and they did not dislocate. This caused copper to flow between fixed diamond particles, which ended up in a compressed copper matrix and mostly unaffected diamond particles. As a result, diamond particles came closer to the surface. Although it is an observed fact that softer copper matrix glides under high pressure while reinforcing hard particles remain their initial ground, it does not confirm emergence of diamond dust on sample surface during CIP. Considering that diamond particles cracked and formed diamond dust is a more reliable explanation.

Scanning electron microscopy images of cold isostatic pressed composite with 75 µm particle size from Fig. 3.20 also confirms that voids at the interfaces are tightly closed. Additionally, the composite thickness is measured 707.8 µm. In both CIP’d samples, the copper morphology has changed. In as deposited sample, the deposited copper was smooth. However, in CIP’d samples it can be seen that copper has sharp ends. The texture has more indentations. This structural change is also related to copper being compressed during isostatic pressing.

Cross-section imaging of CIP’d then annealed sample is given in Fig. 3.21. It is observed that for sample with 250 µm reinforcing particles, the smaller diamond particles which were clearly visible in only CIP’d samples cross-section, are displaced. Other than that, composite structure resembles the CIP’d samples morphology. The texture again has sharp ends and indentations. Annealing afterwards did not alter structural observations of the CIP’d samples.

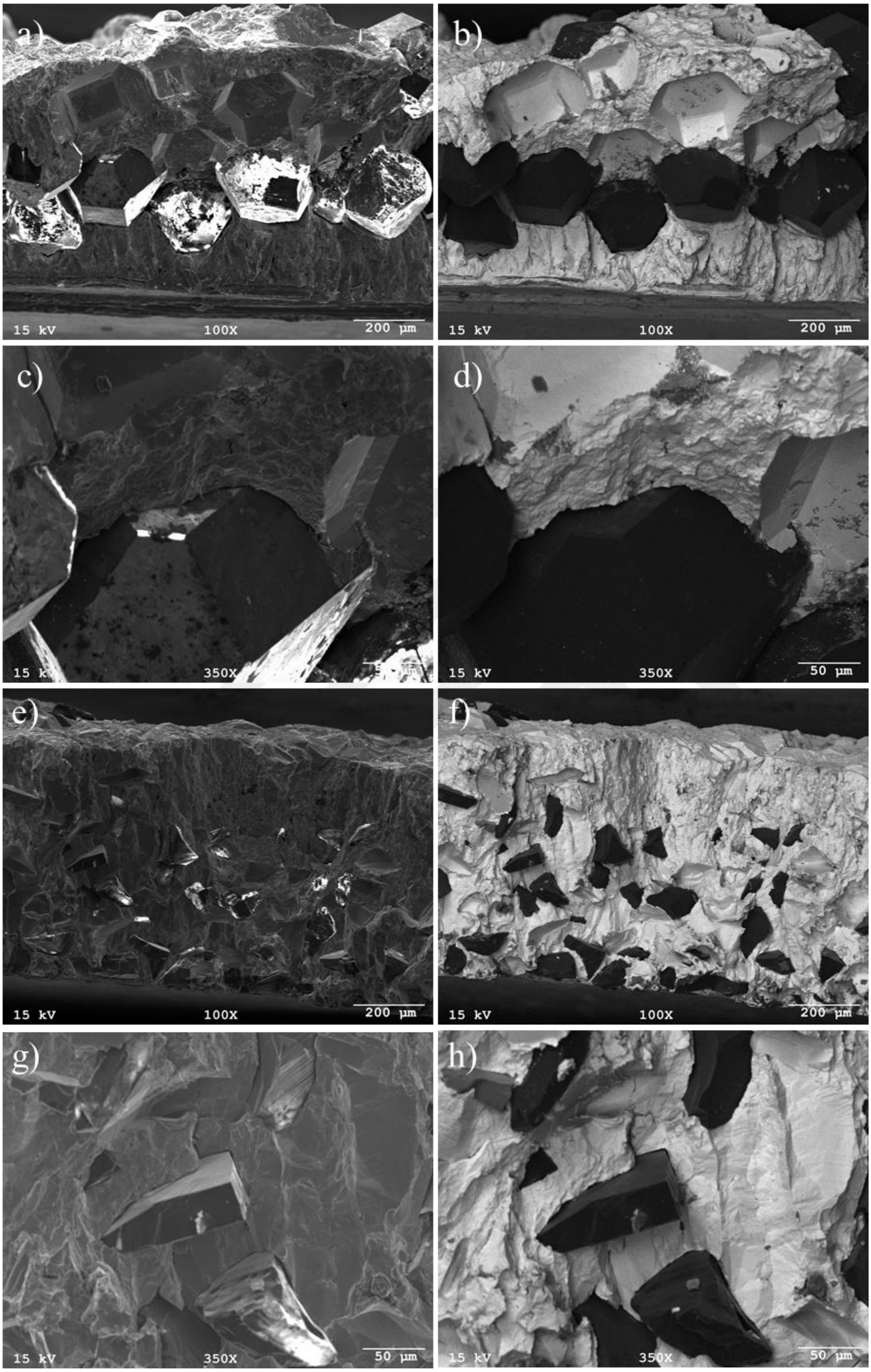
a)
15 kV
100X
200 µm
b)
15 kV
100X
200 µm
c)
15 kV
350X
50 µm
d)
15 kV
350X
50 µm
e)
15 kV
100X
200 µm
f)
15 kV
100X
200 µm
g)
15 kV
350X
50 µm
h)
15 kV
350X
50 µm

Figure 3.21 : SEM images of CIP’d & annealed samples cross-sections, (a,b) at 100X with SE,BSE resp. (c,d) at 350X with SE, BSE resp. (e,f) at 100X with SE, BSE resp. (g,h) at 350X with SE, BSE resp.

3.3.4 Structural Characterization

After fabricating the first succesful diamond coating by 6 hours of electroforming where diamond particles were pinned on substrate surface but they were not covered by pure copper (sample shown in Fig. 3.12), sample is characterized by X-Ray Diffractometer to confirm the identity of the composite. X-Ray diffraction pattern is plotted in gonio mode.

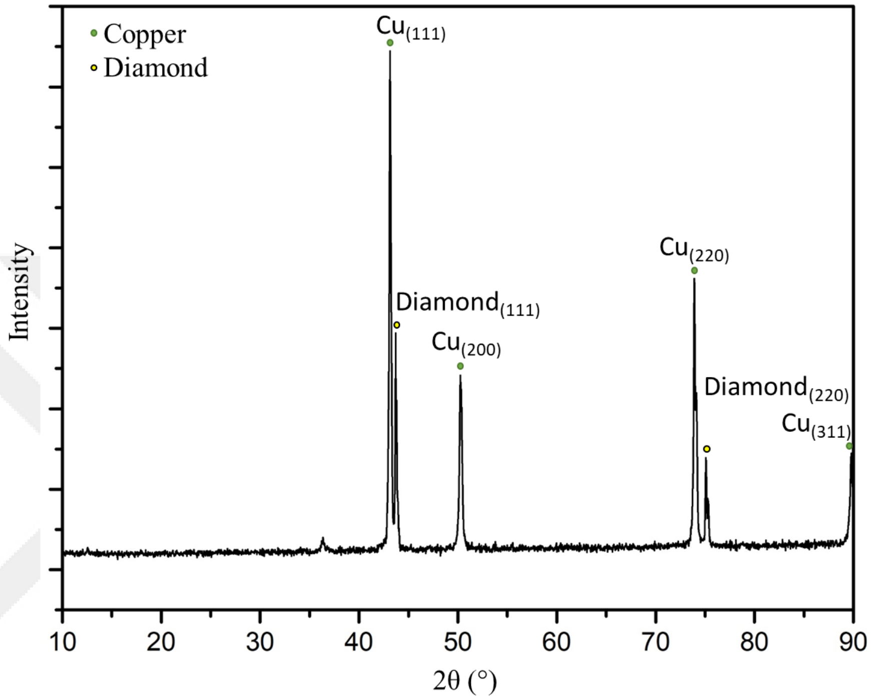

Figure 3.22 : XRD pattern of copper – diamond coating on copper substrate after 6 hours electroforming.

Fig. 3.22 shows the XRD pattern of composite coating. As stated in earlier sections, the reason why this sample is described as a composite plating instead of electroformed composite is related to the fact that; in this sample, diamond particles attached on substrate are not covered by electrodeposited copper but they are pinned on the substrate by a thin copper interface. XRD pattern of fabricated sample matches with the typical patterns of copper-diamond composites in literature [50].

For electroformed composites, in order to analyze the effect of electrodeposition, cold isostatic pressing, annealing and both pressing and annealing on composite structure, X-Ray diffraction patterns of samples with 75 µm particle size is plotted in gonio mode. X-Rays penetrated from the upper surface of the composites. XRD patterns of as deposited and treated samples are given in Fig. 3.23.

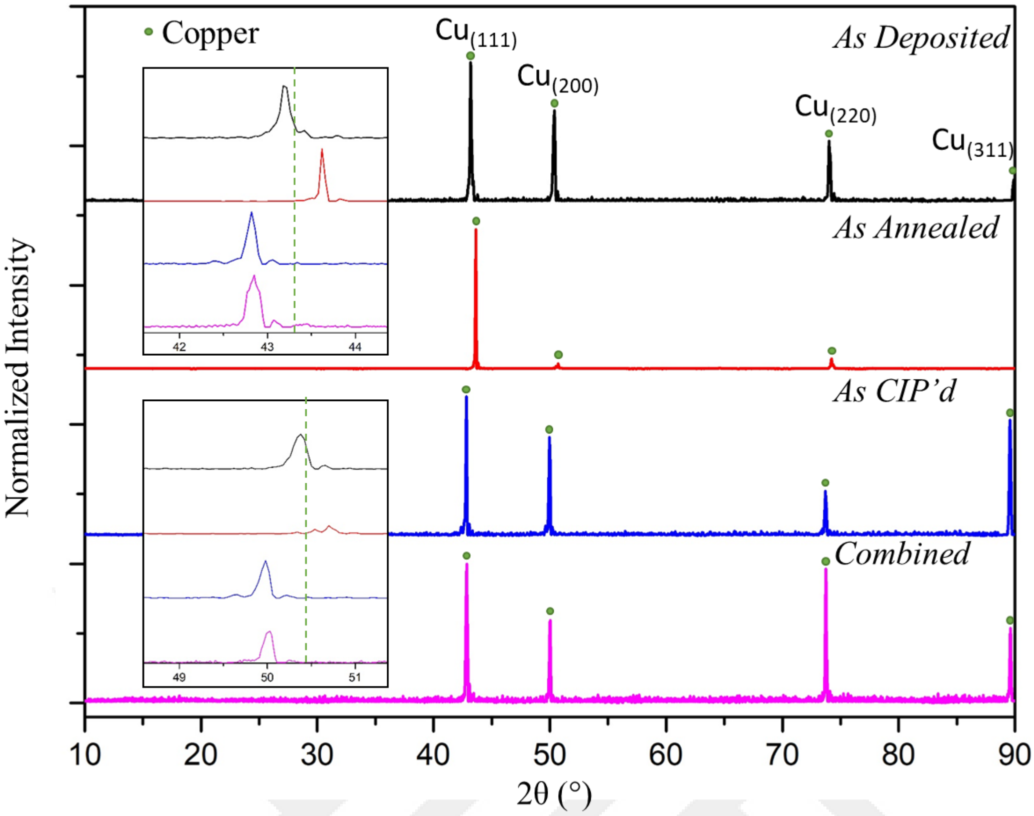

Figure 3.23 : XRD patterns of as deposited, as annealed, as CIP'd and as initially CIP'd then annealed sample (combined) plotted in gonio mode.

The drawback in analyzing XRD patterns of copper – diamond composites is that (111) and (220) planes are both diffraction planes for each material and their peaks may overlap depending on the internal stress build-up. At that point it is troubling to differentiate the diffraction peaks of diamond. Considering that structrual characterization is priorly done to investigate the effect of deposition and post treatments on copper, position of (200) diffraction plane of copper is suitable for a clear observation since (200) is not a diffraction plane for diamond. Yet, as shared in Fig. 3.23, all diffraction planes of copper exhibits the same behaviour. In Fig. 3.23, XRD patterns of as deposited and post treated samples are given with two additional frames focusing on angles 42°-44° and 49°-51° where reference position of copper peaks are marked with a dashed line [58]. Copper peaks of as deposited sample shifted slightly to smaller angles compared to the reference angle, indicating that internal stresses were present. One of the reasons of stress generation is the stresses induced through electrodeposition. Peaks of annealed sample shifted to higher angles. Shared in Table 3.3, (200) plane diffraction angle of annealed copper is 50.70° (2θ), while this angle is 50.38° for as deposited sample. In contrary, after cold isostatic pressing the as deposited sample, relevant angle is measured 49.98°, it shifted to smaller angles again indicating generation of compressive stresses. Annealing of the CIP’d sample recovered the internal stress. (200) planes diffraction angle was this time 50.03°, which is higher than the CIP’d sample but lower than both as deposited and as annealed samples. This situation is also valid for (111) and (220) diffraction planes. Since cold isostatic pressing induces very high compressive stresses along the sample, the angles shifted to smaller angles. It was also noticeable from the SEM images, where copper morphology visibly changed from a smooth structure to sharp and indented structure. Annealing as deposited sample revoked the internal stresses where peaks shifted to larger angles. Annealing CIP’d sample slightly shifted the peak position. Even with annealing the angle of diffraction plane could exceed the diffraction angle of as deposited sample. This indicates that cold isostatic pressing leaves a permanent structural impact, SEM images of combined sample also showed that the morphology of CIP’d sample did not go to a smoother structure after it was annealed.

Table 3.3 : Diffraction planes and corresponding angles for characterized samples.

Sample	Diffraction Plane	2θ (°)
As deposited	(111)	43.16
As deposited	(200)	50.38
As deposited	(220)	74.02
Annealed	(111)	43.62
Annealed	(200)	50,70
Annealed	(220)	74.22
CIP’d	(111)	42.82
CIP’d	(200)	49.98
CIP’d	(220)	73.70
Combined	(111)	42.85
Combined	(200)	50.03
Combined	(220)	73.73
Reference	(111)	43.316
Reference	(200)	50.448
Reference	(220)	74.125

3.3.5 Mechanical characterization

Although the composites can be fabricated near net shape for certain applications through the design of the final product, some application may require complex geometries. In order to satisfy that, the material must have enough formability. It is found that the material was induced with internal stresses during electroforming and annealing removes them. As a mechanical characterization for commenting on formability of materials, three point flexural test was applied to as deposited and as annealed samples. The results of the test are given in Fig. 3.23.

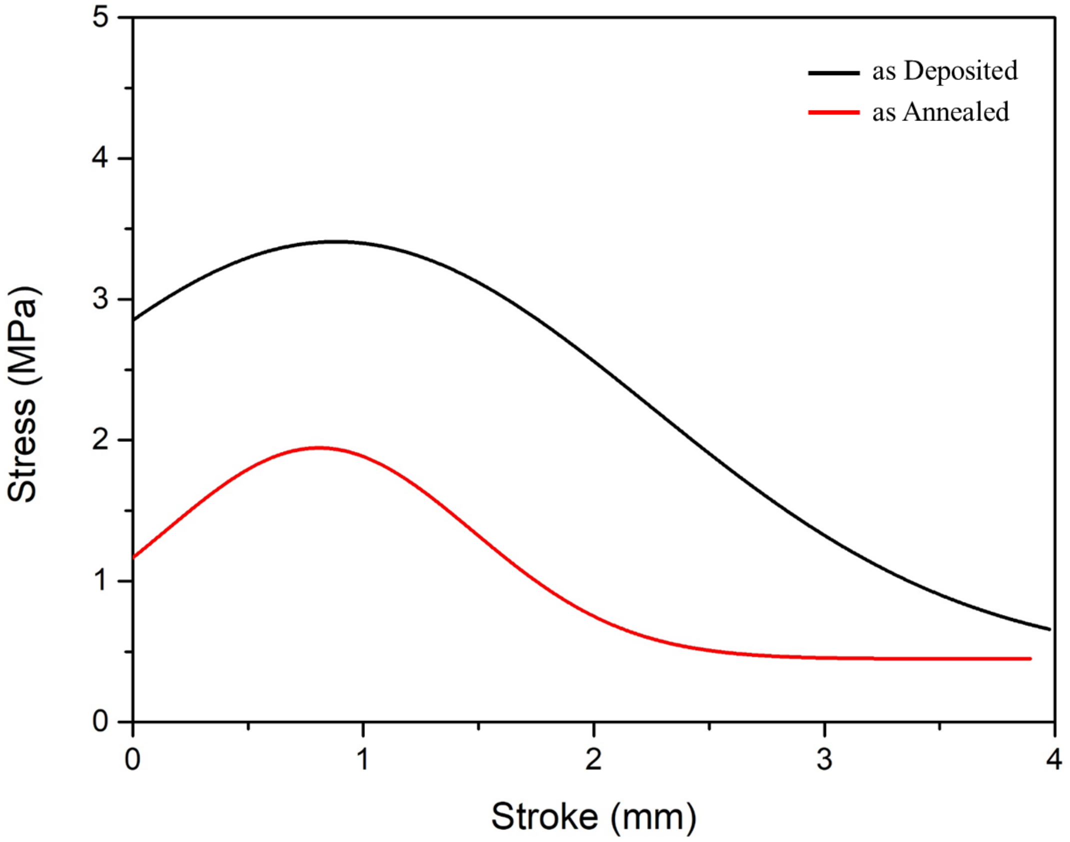

Figure 3.24 : Three point flexural test results of as deposited and as annealed samples.

The stress stroke graph was plotted by using equation 3.1, where F is the load, L, b and d are length, width and thickness of the sample respectively.

$$\sigma = \frac{3FL}{2bd^2} \qquad (3.1)$$

The data obtained from the test was fitted by Origin. In flexural test, the flexural strength corresponds to the stress value while x=0 mm. Flexural strength of as deposited sample is found 2.8 MPa while for annealed sample it is 1.2 MPa. The reason behind the fact that as deposited sample has 2.33 times higher flexural strength than the annealed sample is; at the annealing temperature of 650 °C, grain growth occurred for copper. Hence, grain boundary density was lowered and the material became more ductile. Additionally, annealing removed the internal stresses to a certain extent, which also contributed to enhanced formability.

4. CONCLUSION

Copper-diamond composite material is produced with enhanced reinforcement concentration in metal matrix by method of electroforming. Wetting particles with electrolyte prior to electroforming process prohibited agglomeration of particles and well distributed reinforcement in deposit is obtained since electrolyte with particle surfaces is enabled. Instead of settling particles with conventional SCD technique, in which intermittent agitation is applied, particles settled manually. Higher than 700 μm thicknesses are obtained by conducting electroforming process for 30 hours. By elongating electroforming duration and increasing reinforcement amount that placed on substrate surface, material thickness could be further increased.

Current controlled deposition is not viable in production of composite by electrochemical technique since substrate surface is covered by particles. As process continuous, available surface area changes repeatedly. Surface area dependence of current density causes also change in current density and dendritic deposit morphology is obtained. For that reason deposition control is switched to potential control. Current density-potential curve of electroforming electrolyte is obtained by using a potentiostat. Potential difference required for achieving a corresponding current density of 1 A/dm^2 is found as 160 mV. Potential difference between anode and cathode with a magnitude that fixes potential difference at 160 mV between working electrode and copper reference electrode is achieved by applying a steady 300 mV potential from the power supply.

Composite material that is produced by 30 hours electroforming duration was nondestructively detachable from the substrate by a little manual force application. Therefore in production by electroforming technique any further electrochemical or mechanical processes is no longer required to obtain a self-standing composite material.

SEM images of cross sections of as deposited copper-diamond composite showed that, the interface was nearly void free and satisfying. However for further improved interfacial properties effects of cold isostatic pressing and cold isostatic pressing followed by annealing are investigated. Any effect of annealing on interface is not observed. Cold isostatic pressing however had distinct effects on composite. SEM images of cold isostatic pressed samples indicate that voids at interfaces were eliminated. After cold isostatic pressing copper morphology changed itself to an indented structure.

EDS analysis indicated that any undesired impurities were not present in composite.

XRD patterns of as deposited samples showed that copper peaks were shifted to lower angles. It is an expected result due to compressive stresses introduced to the structure during electroforming process. When samples are annealed, peaks shifted towards their original positions because annealing removed the compressive stresses that arose from deposition. Cold isostatic pressing shifted peaks to smaller angles indicating high compressive stress generation. For cold isostatic pressed and then annealed samples a lowering in compressive stresses is observed when compared to cold pressed samples. However, for the annealing duration used in this study a complete recovery of the stresses is not attained.

Three point flexural strength test results indicates that annealing decreases flexural strength of material. As deposited sample has a flexural strength of 1.2 Mpa, whereas flexural strength of annealed sample is 2.8MPa.

Copper-diamond composite material having reliable interface, high diamond content and void free structure is producible in desired shape and dimensions with electroforming method.

REFERENCES

[1] **Almubarak, A.** (2017). The Effects of Heat on Electronic Components. *International Journal of Engineering Research and Applications*, *07*(05), 52–57.

[2] **Kitzmantel, M., & Neubauer, E.** (2015). Innovative hybrid heat sink materials with high thermal conductivities and tailored CTE. *Components and Packaging for Laser Systems*, *9346*(March 2017), 934606.

[3] **Kidalov, S. V., & Shakhov, F. M.** (2009). Thermal conductivity of diamond composites. *Materials*, *2*(4), 2467–2495.

[4] **Chung, L.** (2010). *Composite Materials*. In *Engineering Materials and Processes*: *Vol. 91*.

[5] **Chitode, J.** (2009). *Power electronics*. Pune, India: Technical Publications Pune.

[6] **Alaoui, C.** (2011). *Testing and Simulation of Solid State Heating and Cooling*. *3*(2), 1636–1641.

[7] **Ahmed, H. E., Salman, B. H., Kherbeet, A. S., & Ahmed, M. I.** (2018). Optimization of thermal design of heat sinks: A review. *International Journal of Heat and Mass Transfer*, *118*, 129–153.

[8] **Ong, K. S., Tan, C. F., Lai, K. C., & Tan, K. H.** (2017). Heat spreading and heat transfer coefficient with fin heat sink. *Applied Thermal Engineering*, *112*(September), 1638–1647.

[9] **Jouhara, H., Chauhan, A., Nannou, T., Wrobel, L. C.** (2017). Heat pipe based systems - Advances and applications. *Energy*, *128*, 729–754.

[10] **Böckh, P., & Wetzel, T.** (2012). *Heat Transfer Basics and Practice*. Berlin, Heidelberg: Springer, pp. 1-9

[11] **Teraji, T., Taniguchi, T., Koizumi, S., Isoya, J.** (2012). Chemical vapor deposition of 12C isotopically enriched polycrystalline diamond. *Japanese Journal of Applied Physics*, *51*(9).

[12] **Schleuning, D., Scholz, K., Griffin, M., Hasenberg, T.** (2009). Material survey for packaging semiconductor diode lasers. *High-Power Diode Laser Technology and Applications VII*, *7198*(July 2014), 71981K.

[13] **Abyzov, A. M., Kidalov, S. V., & Shakhov, F. M.** (2012). High thermal conductivity composite of diamond particles with tungsten coating in a copper matrix for heat sink application. *Applied Thermal Engineering*, *48*, 72–80.

[14] **Bai, G., Zhang, Y., Dai, J., Zhang, H.** (2019). Tunable coefficient of thermal expansion of Cu-B/diamond composites prepared by gas pressure infiltration. *Journal of Alloys and Compounds*, *794*, 473–481.

[15] **Cho, H. J., Kim, Y. J., & Erb, U.** (2018). Thermal conductivity of copper-diamond composite materials produced by electrodeposition and the effect of TiC coatings on diamond particles. *Composites Part B: Engineering*, *155*, 197–203.

[16] **Cho, H. J., Yan, D., Tam, J., & Erb, U.** (2019). Effects of diamond particle size on the formation of copper matrix and the thermal transport properties in electrodeposited copper-diamond composite materials. *Journal of Alloys and Compounds*, *791*, 1128–1137.

[17] **Jia, J., Bai, S., Xiong, D., Chang, J.** (2019). Effect of tungsten based coating characteristics on microstructure and thermal conductivity of diamond/Cu composites prepared by pressueless infiltration. *Ceramics International*, *45*(8), 10810–10818.

[18] **Kang, Q., He, X., Ren, S., Qu, X.** (2013). Preparation of copper-diamond composites with chromium carbide coatings on diamond particles for heat sink applications. *Applied Thermal Engineering*, *60*(1–2), 423–429.

[19] **Li, J., Zhang, H., Zhang, Y., Wang, X.** (2015). Microstructure and thermal conductivity of Cu/diamond composites with Ti-coated diamond particles produced by gas pressure infiltration. *Journal of Alloys and Compounds*, *647*, 941–946.

[20] **Chandra Kandpal, B., Kumar, J., & Singh, H.** (2018). Manufacturing and technological challenges in Stir casting of metal matrix composites- A Review. *Materials Today: Proceedings*, *5*(1), 5–10.

[21] **Clyne, T. W., & Withers, P. J.** (1993). *An Introduction to Metal Matrix Composites*.

[22] **Annigeri, U. K., & Veeresh Kumar, G. B.** (2017). Method of stir casting of Aluminum metal matrix Composites: A review. *Materials Today: Proceedings*, *4*(2), 1140–1146.

[23] **Thandalam, S. K., Ramanathan, S., & Sundarrajan, S.** (2015). Synthesis, microstructural and mechanical properties of ex situ zircon particles (ZrSiO4) reinforced Metal Matrix Composites (MMCs): A review. *Journal of Materials Research and Technology*, *4*(3), 333–347.

[24] **Kalemtaş, A.** (2016). *İnfiltrasyon Yöntemiyle Kompozit Üretiminde Etkili Olan Temel Değişkenler*.

[25] **Michaud, V., & Mortensen, A.** (2001). Infiltration processing of fibre reinforced composites: Governing phenomena. *Composites - Part A: Applied Science and Manufacturing*, *32*(8), 981–996.

[26] **Dong, Q., Chen, L. Q., Zhao, M. J., & Bi, J.** (2004). Synthesis of TiCp reinforced magnesium matrix composites by in situ reactive infiltration process. *Materials Letters*, *58*(6), 920–926.

[27] **Jahromi, S. S.** (2019). *The production and sustainable role of particle composites in engineering structures*. (June), 0–12.

[28] **Garg, P., Jamwal, A., Kumar, D., Gupta, P.** (2019). Advance research progresses in aluminium matrixcomposites: Manufacturing & applications. *Journal of Materials Research and Technology*, *8*(5), 4924–4939.

[29] **Evans, A., San Marchi, C., & Mortensen, A.** (2003). *Metal Matrix Composites in Industry*.

[30] **Dong, Y., Zhang, R., He, X., Qu, X.** (2012). Fabrication and infiltration kinetics analysis of Ti-coated diamond/copper composites with near-net-shape by pressureless infiltration. *Materials Science and Engineering B: Solid-State Materials for Advanced Technology*, *177*(17), 1524–1530.

[31] **Park, S. J., & Seo, M. K.** (2011). Solid-Liquid Interface. In *Interface Science and Technology* (Vol. 18).

[32] **Sinha, V., & Spowart, J. E.** (2013). Influence of interfacial carbide layer characteristics on thermal properties of copper-diamond composites. *Journal of Materials Science*, *48*(3), 1330–1341.

[33] **Schubert, T., Ciupiński, Zieliński, W., Kieback, B.** (2008). Interfacial characterization of Cu/diamond composites prepared by powder metallurgy for heat sink applications. *Scripta Materialia*, *58*(4), 263–266.

[34] **Shen, X. Y., He, X. B., Ren, S. Bin, Qu, X. H.** (2012). Effect of molybdenum as interfacial element on the thermal conductivity of diamond/Cu composites. *Journal of Alloys and Compounds*, *529*, 134–139.

[35] **Xia, Y., Song, Y., Qing, L., C. Guang.,** (2009). Effect of carbide formers on microstructure and thermal conductivity of diamond-Cu composites for heat sink materials. *Transactions of Nonferrous Metals Society of China (English Edition)*, *19*(5), 1161–1166.

[36] **Zhang, Y., Zhang, H. L., Wu, J. H., & Wang, X. T.** (2011). Enhanced thermal conductivity in copper matrix composites reinforced with titanium-coated diamond particles. *Scripta Materialia*, *65*(12), 1097–1100.

[37] **Chu, K., Liu, Z., Jia, C., Guo, H.** (2010). Thermal conductivity of SPS consolidated Cu/diamond composites with Cr-coated diamond particles. *Journal of Alloys and Compounds*, *490*(1–2), 453–458.

[38] **Bai, H., Ma, N., Lang, J., Ma, Y.** (2013). Thermal conductivity of Cu/diamond composites prepared by a new pretreatment of diamond powder. *Composites Part B: Engineering*, *52*, 182–186.

[39] **Raza, K., & Khalid, F. A.** (2014). Optimization of sintering parameters for diamond-copper composites in conventional sintering and their thermal conductivity. *Journal of Alloys and Compounds*, *615*, 111–118.

[40] **Ren, S., Shen, X., Guo, C., Qu, X.** (2011). Effect of coating on the microstructure and thermal conductivities of diamond-Cu composites prepared by powder metallurgy. *Composites Science and Technology*, *71*(13), 1550–1555.

[41] **Bai, G., Wang, L., Zhang, Y., Zhang, H.** (2019). Tailoring interface structure and enhancing thermal conductivity of Cu/diamond composites by alloying boron to the Cu matrix. *Materials Characterization*, *152*(April), 265–275.

[42] **Ciupiński, Ł., Kruszewski, M. J., Grzonka, J., Michalski, A.** (2017). Design of interfacial Cr3C2 carbide layer via optimization of sintering parameters used to fabricate copper/diamond composites for thermal management applications. *Materials and Design*, *120*, 170–185.

[43] **Kanani, N.** (2004). *Electroplating: Basic Principals, Processes and Practice*. Bodmin: Elsevier.

[44] **Walsh, F. C., & Ponce de Leon, C.** (2014). A review of the electrodeposition of metal matrix composite coatings by inclusion of particles in a metal layer: an established and diversifying technology. *Transactions of the IMF*, *92*(2), 83–98.

[45] **Guglielmi, N.** (1972). *Kinetics of the Deposition of Inert Particles from Electrolytic Baths*. *1501*(8), 1009–1012.

[46] **Celis, J. P.** (1987). A Mathematical Model for the Electrolytic Codeposition of Particles with a Metallic Matrix. *Journal of The Electrochemical Society*, *134*(6), 1402.

[47] **Hovestad, A., & Janssen, L. J. J.** (1995). Electrochemical codeposition of inert particles in a metallic matrix. *Journal of Applied Electrochemistry*, *25*(6), 519–527.

[48] **Berçot, P., Pea-Muoz, E., & Pagetti, J.** (2002). Electrolytic composite Ni-PTFE coatings: An adaptation of Guglielmi’s model for the phenomena of incorporation. *Surface and Coatings Technology*, *157*(2–3), 282–289.

[49] **Yeh, S. H., & Wan, C. C.** (1994). Codeposition of SiC powders with nickel in a Watts bath. *Journal of Applied Electrochemistry*, *24*(10), 993–1000.

[50] **Yoshida, K., & Morigami, H.** (2004). Thermal properties of diamond/copper composite material. *Microelectronics Reliability*, *44*(2), 303–308.

[51] **Pushpavanam, M., Manikandan, H., & Ramanathan, K.** (2007). Preparation and characterization of nickel-cobalt-diamond electro-composites by sediment co-deposition. *Surface and Coatings Technology*, *201*(14), 6372–6379.

[52] **Ghouse, M.** (1980). Electrocodeposited composites of graphite, molybdenum disulfide with copper for tribological applications. *Metal Finishing*, *78*(11, 1980), 55–60.

[53] **Sun, Y., Flis-Kabulska, I., & Flis, J.** (2014). Corrosion behaviour of sediment electro-codeposited Ni-Al2O 3 composite coatings. *Materials Chemistry and Physics*, *145*(3), 476–483.

[54] **S.Jeyaraj; R.Saravanan; K.P.Arulshri; G.muralidharan**. (2015). Effect studies on Electrodeposited Ni- Al_2O_3.pdf. *International Journal of Engineering and Technical Research (IJETR)*, (3), 390–397. Retrieved from 390 www.erpublication.org

[55] **Maurin, G., & Lavanant, A.** (1995). Electrodeposition of nickel/silicon carbide composite coatings on a rotating disc electrode. *Journal of Applied Electrochemistry*, *25*(12), 1113–1121.

[56] **Zhang, X., Qin, J., Das, M. K., Liu, R.** (2016). Co-electrodeposition of hard Ni-W/diamond nanocomposite coatings. *Scientific Reports*, *6*(November 2014), 1–11.

[57] **Qin, J., Zhang, X., Xue, Y., Liu, R.** (2015). The high concentration and uniform distribution of diamond particles in Ni-diamond composite coatings by sediment co-deposition. *Surface and Interface Analysis*, *47*(3), 331–339.

[58] **Otte, H. M.** (1961). Lattice parameter determinations with an X-ray spectrogoniometer by the debye-scherrer method and the effect of specimen condition. *Journal of Applied Physics*, *32*(8), 1536–1546.

CURRICULUM VITAE

Name Surname : Gökçe EVREN

Place and Date of Birth : Bartın, 27.01.1993

E-Mail : gokcemtl@gmail.com

EDUCATION :

- **B.Sc.** : 2017, Istanbul Technical University, Faculty of Chemistry and Metallurgy, Metallurgical and Materials Engineering
- **Highschool** : 2011, Bartın Fen Lisesi

PROFESSIONAL EXPERIENCE AND REWARDS:

- 2019, Research Assistant, Turkish-German University, Department of Materials Science and Technologies
- 2016, Componenta Döktaş Dökümcülük, Orhangazi / Bursa, Internship
- 2015, Mescier Demir Çelik San. Tic. Ltd. Şti., Bartın, Management Internship
- 2013, Barmak San. Tic. Ltd. Şti, Bartın, Atelier Internship